EMU
Journal of
Pharmaceutical
Sciences

ISSN: 2651-3587
Volume 8 / Issue 3

EMUJPharmSci

December 2025

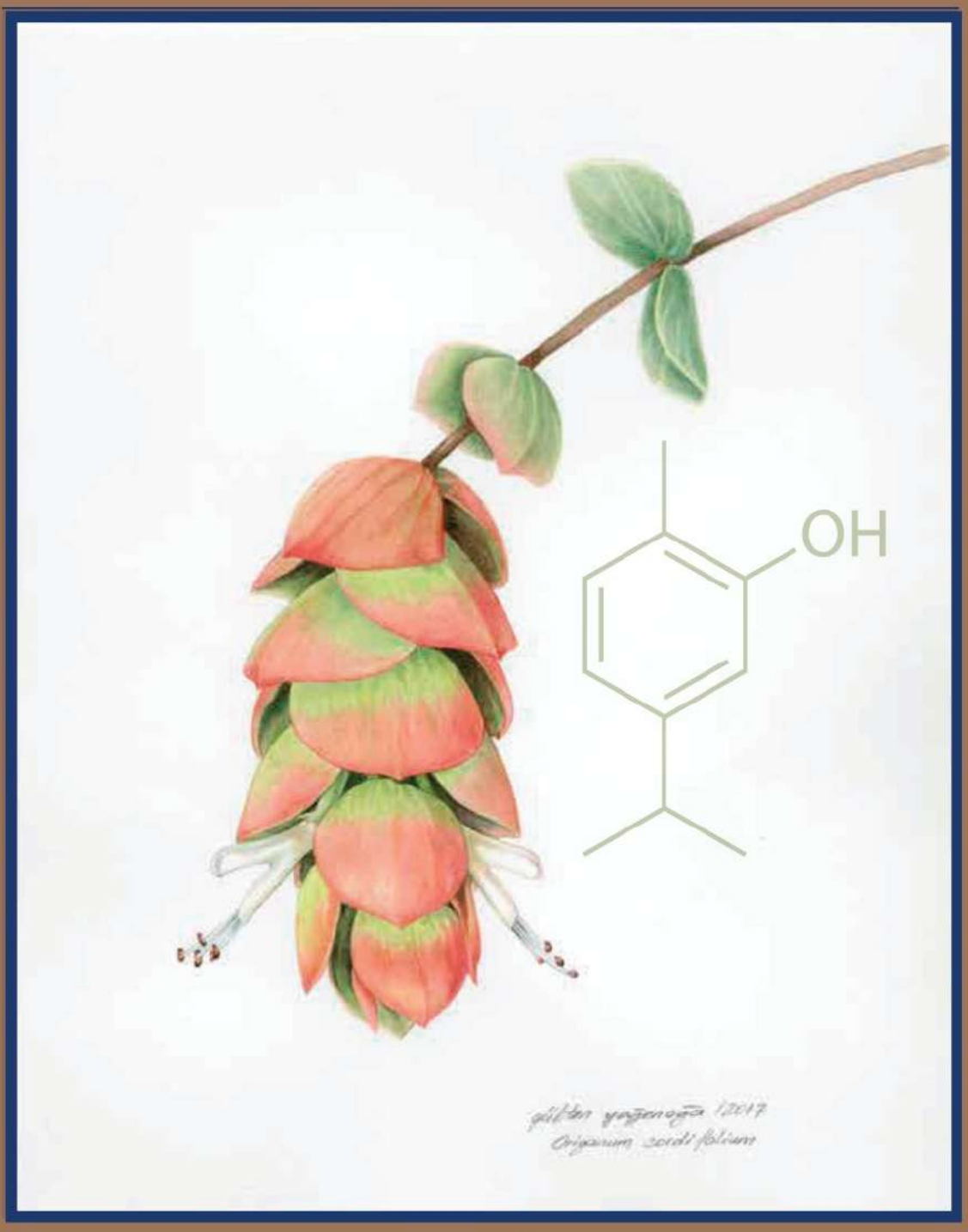

Eastern Mediterranean University Press

EDITORIAL BOARD

Origanum cordifolium* **in cover picture was illustrated by Gülten Yeğenağa

EMU
Journal of
Pharmaceutical
Sciences

EMUJPharmSci

Advisory/Scientific Board

EMU
Journal of
Pharmaceutical
Sciences
EMUJPharmSci

MESSAGE FROM THE EDITOR IN CHIEF

Dear Colleagues,

Finally, we have reached to the end of 2025. The EMU Journal of Pharmaceutical Sciences Editorial, and Scientific/Advisory Board wish you a beautiful new year. We are also very proud to introduce the final, 3rd issue of the year.

This issue features several interesting research articles from diverse university centers and laboratories. The effects of *Rosmarinus officinalis* against certain bacteria, the design, synthesis, and biological activities of substituted propanhydrazide derivatives, HPLC method development for butenafine-curcumin containing preparations, as well as computational studies on HSP90 inhibitors from herbal sources are expected to attract the attention of researchers in the relevant fields. The review article provides comprehensive insights into updates on chemotherapy and personalized medicine.

As a member of 'DergiPark Akademik,' an establishment under the Scientific and Technological Research Council of Türkiye (TÜBİTAK), EMU Journal of Pharmaceutical Sciences continues its journey with a transparent peer-review and publication process for scientific studies across diverse fields related to pharmaceutical sciences. The journal remains committed to promoting the global dissemination of pharmaceutical research, providing a platform for scientists worldwide. It is important to note that the journal does not charge any submission or acceptance fees.

We look forward to your scientific contributions,

Best wishes,

Prof. Dr. H. Ozan Gülcan

Dean of Faculty of Pharmacy
Editor in Chief
Eastern Mediterranean University
Faculty of Pharmacy
Famagusta, TRNC, via Mersin 10, Türkiye

EMU
Journal of
Pharmaceutical
Sciences
EMUJPharmSci

GUIDE FOR AUTHORS

EMU Journal of Pharmaceutical Sciences (EMUJPharmSci) publishes research on all aspects of pharmacy in the form of original articles, short reports, and reviews.

EMU Journal of Pharmaceutical Sciences is published three times each year. It is an open-access, peer-reviewed journal.

- Contributions to EMU Journal of Pharmaceutical Sciences must be in English.
- All manuscripts are subject to editorial review.
- Manuscripts should not have been previously published or accepted for publication and must not be submitted simultaneously to other journals.
- The manuscripts are published in the order of final acceptance after review and revision.
- If a manuscript is returned to the authors for revision and the revised version is not received by the editor within 2 months, it will be treated as a new submission.
- If the manuscript is accepted and the proof is returned to the authors, corrected proofs should be sent to the editor within 5 days.

Original Articles: These are limited to 15 typewritten pages, in addition to supplementary materials (schemes, tables, figures, etc.).

Short Papers: Short papers are limited to 5 typewritten pages, with a maximum of 2 supplementary materials (schemes, tables, figures).

Reviews: Reviews are limited to 20 pages, in addition to supplementary materials (schemes, tables, figures, etc.).

- The original manuscript must be arranged as follows: Title page (including the title, authors and correspondence address), abstract, key words, introduction, materials and methods, results and discussion, acknowledgements and references.
- Reviews must be arranged as follows: Title page (including the title, authors, and correspondence address), abstract, introduction, discussion, acknowledgements, and references.

EMU Journal of Pharmaceutical Sciences
EMUJPharmSci

1. General Format

a) All manuscripts can only be submitted electronically via DergiPark.
b) Manuscripts should be 1.5-lines spaced and justified.
c) Use 2.5 cm margins and Times New Roman font on A4 paper.
d) Number all pages, starting with the title page.
e) Spell out all acronyms in full at first use.
f) Make sub-headings if necessary.
g) Follow internationally accepted rules and conventions: use the international system of units (SI).

2. Before main text

A. Title page

a) The first page of the manuscript is a title page containing the following information:
b) The manuscript's full title (*Font: Times New Roman Font Size: 13*). The title must be concise and informative.
c) All authors' full names (*Font: Times New Roman Font Size: 11)*.
d) The affiliation of the author(s) should be linked by superscript numbers, and listed beneath the title.
e) All authors' ORCID ID number (*Font: Times New Roman Font Size: 11)*.
f) Corresponding author (*Font: Times New Roman Font Size: 10)*. E-mail, telephone and fax number (with country and area code) of the corresponding author should be provided.
g) Ethical approval must be provided for studies involving human or animal participants.

B. Abstract

a) The abstract appears on its own page.
b) The abstract should be written in Times New Roman and font size 11.
c) The maximum length of the abstract is 200 words.
d) The abstract should contain the objectives, methods, results and conclusions.
e) 3- 6 key words must be provided in alphabetical order (Font: Times New Roman Font Size: 10). Separate keywords with commas.

3. Main text

A. Introduction

(Font: Times New Roman Font Size: 12)
State the objectives of the work and provide a brief background of the literature related to the topic. The novelty and the aim of the study should be clearly stated.

B. Materials and Methods

(Font: Times New Roman Font Size: 12)
a) Give a brief and clear description of the materials and methods used. Subtitles can be given as appropriate.
b) For plant materials, herbarium name (or acronym), number, name and surname of the person who identified the plant materials should be indicated in this part of the manuscript.
c) Statistical analysis must be provided when necessary

EMU Journal of Pharmaceutical Sciences
EMUJPharmSci

C. Results and Discussion

(Font: Times New Roman Font Size: 12)

A combined Results and Discussion section is often appropriate. Results should be concise.

Discussion should explore the significance of the results of the work.

Discussion should not repeat the results.

The main conclusions of the study should be presented.

D. Acknowledgement

(Font: Times New Roman Font Size: 10)

Supporting institutions or individuals should be briefly acknowledged just before the reference list.

E. References

i. Citation in text

(Font: Times New Roman Font Size: 12)

- Please ensure that every reference cited in the text is also present in the reference list (and vice versa).
- Unpublished results and personal communications are not recommended in the reference list.
- References in the text should be cited as: the author(s) surname and the publication date**.**

Examples:

(Sahin, 2000) – one author

(Sahin and Kosar, 2000) – Two authors

(Sahin et al., 2000) – more than two authors

(Celik and Ozhatay 2000 a, b) – More than one paper in the same year by the same author (s)

(Ozhatay and Avci, 2000; Ozhatay et al., 2001; Ozhatay, 2005) – listed by the earliest year first for multiple citations.

ii. Reference style

(Font: Times New Roman Font Size: 10)

- The list of references should be single-spaced.
- List the references in alphabetical order under section of "references".
- For references up to 5 authors, write the names of all authors.
- For references more than 5 authors, write the names of the first 5 and add et al.
- The title of journal should be abbreviated in italics according to the style used in the National Library of Medicine's Journals in NCBI Databases.
- Volume numbers should be indicated in bold letters.

iii. Examples

Reference to a journal publication:

Ozhatay N, Kultur S, Gurdal B (2017). Check-list of additional taxa to the supplement flora of Türkiye VIII. *Istanbul J Pharm* **47**(1): 31-46.

Ozhatay N, Kultur S, Gurdal B, Ilktac M, Ogmen S, et al. (2019). Check-list of additional taxa to the supplement flora of Türkiye X. *Istanbul J Pharm* **57**(2): 35-46.

Reference to a book:

Strunk W Jr, White EB (1979). The Elements of Style. 3rd ed. New York, NY: Macmillan.

Reference to a chapter in an edited book:

Bonati A (1988). Industry and conservation of medicinal plants. In Akerele O, Heywood V, Synge H (eds). The Conservation Medicinal Plants p.141-148 Cambridge University Press UK.

Electronic resources:
World Nuclear Association (WNA) (2014). Radioisotopes in Medicine, http://www.world-nuclear.org/info/ Accessed 13.10.2014.

4. After main text

Figures / Tables captions

- Use figures and tables for information better presented visually.
- All the figures and tables must be referred to in the main body of the text.
- Tables and Figures should be numbered consequently in the order of appearance within the text, referred as “Table 1” and “Figure 1”.
- Descriptive titles should be given at the top of the tables and at the bottom of the figures.
- Figures should be prepared with the highest resolution and should be provided as a separate page following references.

Submission checklist

Check the following submission list before submit your manuscript:

- Full E-mail address, full postal address, telephone and fax number of the corresponding author.
- All necessary files have been uploaded.
- References are in the correct format for this journal.
- All references mentioned in the Reference list are cited in the text.
- All figure captions.
- All tables (including title, description, footnotes).

For any further information please e-mail: emuj.pharmsci@emu.edu.tr

EMU
Journal of
Pharmaceutical
Sciences
EMUJPharmSci

CONTENTS

Research articles

Reviews

Research Article EMUJPharmSci ISSN 2651-3587 https://dergipark.org.tr/emujpharmsci

EMU Journal of Pharmaceutical Sciences

EMUJPharmSci

Anti-inflammatory and Antibacterial Activities of *Rosmarinus officinalis* L. Essential Oil and Hydrosol against *Methicillin-Resistant Staphylococcus aureus*

Goksu Oduncuoglu[1]*, Gizem Sanlitürk[1]

[1]Bahcesehir Cyprus University, Faculty of Pharmacy, Nicosia, North Cyprus via Mersin 10, Türkiye.

Abstract

Rosmarinus officinalis L. (Rosemary), recently reclassified as *Salvia rosmarinus* Spenn., grows endogenously in the Mediterranean region. The essential oil of rosemary has been demonstrated to have anti-inflammatory, antibacterial, and antioxidant activities. The present study aimed to evaluate the anti-inflammatory and antibacterial activities of the essential oil and hydrosol of *R. officinalis* against methicillin-resistant *staphylococcus aureus* (MRSA). The aerial parts of *R. officinalis* were collected in Altınova, Iskele, North Cyprus and hydro-distillation method was performed using a Clevenger apparatus to obtain the essential oil and the hydrosol. Anti-inflammatory activity of the oil (25-200 µg/ml) was evaluated using the protein denaturation inhibition assay. The antibacterial activity of the oil and the hydrosol was tested against MRSA ATCC 33591 using the well diffusion method. Experiments were carried out in triplicate, and statistical analysis was performed using the Chi-square test. The oil showed concentration-dependent anti-inflammatory activity (3.07 ± 0.296% to 32.46 ± 2.229% at 25-200 µg/ml, $p<0.05$). The essential oil and the hydrosol of *R. officinalis* had moderate antibacterial activity against MRSA with the inhibition zones of 13.6 ± 1.154 mm and 16.6 ± 1.527 mm, respectively. The anti-inflammatory and antibacterial activities are attributed to the presence of active compounds 1,8-cineole, α-pinene, camphene and camphor. These products may serve as promising alternatives or complements to conventional medicine for combating resistant bacteria.

Keywords

Anti-inflammatory, antibacterial, essential oil, hydrosol, MRSA, *Rosmarinus officinalis.*

Article History

Submitted: 24 November 2025 Accepted: 11 December 2025 Published Online: December 2025

Article Info

***Corresponding author:** Goksu Oduncuoglu **email:** goksu.oduncuoglu@baucyprus.edu.tr

Research Article:
Volume: 8 Issue: 3 Pages: 124-131
DOI: 10.54994/emujpharmsci.1827520

INTRODUCTION

Rosmarinus officinalis L. (Rosemary) which is recently known as *Salvia rosmarinus* Spenn belongs to Lamiaceae family and endogenously grows in Mediterranean region. Rosemary extract and its essential oil have various usages in pharmaceutical, cosmetics and food industries. It has been used as a food preservative and spicing of the food (Couto et al. 2012). In addition, rosemary essential oil is one of the fragrances in perfumery industry and used in cosmetics as a skin conditioning and brightening agents. The essential oil of *R. officinalis* has been demonstrated to have biological activities such as anticancer, anti-inflammatory, antidiabetic, antioxidant and antibacterial activity against different bacterial strains (Annemer et al. 2022). Antibacterial activity is generally related to the phytochemical composition of the oil. The chemical composition analyses of the essential oil have shown the presence of bioactive compounds such as 1,8-cineole, α-pinene, camphene, and camphor are the major compounds which are thought to be responsible for antibacterial activity (Kabotso et al. 2024). The essential oil that has been tested against different strains, *Escherichia coli, Klebsiella pneumoniae, Staphylococcus aureus,* and *Pseudomonas aeruginosa,* was reported to have antibacterial effective (Annemer et al. 2022).

Staphylococcus aureus is a Gram-positive bacterium that can cause various illnesses ranging from mild to life-threatening consequences in humans (El Aila et al. 2017). Methicillin-resistant *S. aureus* (MRSA) is resistant to many conventional antibiotics (Kim et al. 2018). Vancomycin remains one of the last options for treating MRSA-related infections. In 2019, it was reported that MRSA-related infections caused approximately 121,000 deaths globally (An et al. 2024). Therefore, there is an urgent need for alternative antibacterial agents and complementary medicines, particularly against MRSA infections.

This study investigated anti-inflammatory and antibacterial activities of *R. officinalis* essential oil and hydrosol and their potential role in fighting against MRSA infections.

MATERIALS AND METHODS

Collection of *Rosmarinus officinalis L.*

Aerial parts of *Rosmarinus officinalis* L. were collected from Altınova, İskele, North Cyprus (Figure 1). The plant sample was authenticated by Asst. Prof. Dr. Goksu Oduncuoglu and the specimen was deposited with the Voucher number: BAU/PHARM/LAMI/003 in Bahcesehir Cyprus University, Faculty of Pharmacy. First, the aerial parts were cleaned of unwanted and damaged leaves. The remaining samples were shade-dried at room temperature and then chopped into small pieces. The pieces were then ground and weighed. The essential oil and hydrosol were obtained with the hydro-distillation method using a Clevenger-type apparatus for 3h. After distillation, the oil layer was separated from the hydrosol, and both the oil and hydrosol were stored in the refrigerator at 4 °C for further studies.

Figure 1: *Rosmarinus officinalis* L. photographed in its natural habitat in Cyprus. Photographer: C. S. Christodoulou and G. N. Hadjikyriakou (Hand et al. 2011).

Anti-inflammatory activity of *Rosmarinus officinalis* L. essential oil

The anti-inflammatory activity of the oil of *Rosmarinus officinalis* L. was tested using bovine serum albumin (BSA) denaturation assay (Bhat et al. 2022). BSA solution (1%) was prepared, and pH was adjusted to 6.3. The solution was added to diclofenac sodium (standard control) and rosemary essential oil (25-200 µg/ml) in 1:9 ratio. Rosemary oil was dissolved in methanol to adjust the concentrations. The mixture was heated (57ºC) and allowed to cool down at room temperature. The absorbance was measured at 660 nm using UV/VIS spectrometer and the percentage inhibition of protein denaturation was calculated using the formula (Bhat et al. 2022);

% inhibition of protein denaturation = $\frac{Absorbance\ of\ control - Absorbance\ of\ sample}{Absorbance\ of\ control}$ x 100

Antibacterial activity of *Rosmarinus officinalis* L. essential oil and hydrosol

The antibacterial activity of the oil and hydrosol of *Rosmarinus officinalis* L. was performed using the agar well diffusion assay against MRSA (ATCC 33591) (Talib et al. 2020). The inhibition zones were measured in millimeters. Preparation of the bacterial suspension was done using McFarland 0.5 standard, which corresponds to $1.5x10^8$ CFU/mL. Firstly, the bacterial solution was spread onto the agar surface. Afterwards, wells with a diameter of 6 mm were prepared. Then, the oil and hydrosol of *Rosmarinus officinalis* L. were added into separate wells. The agar plates were incubated at 37 °C for 24 hours. All experiments were performed in triplicate. Gallic acid was used as the positive control.

Statistical analysis

The experiments were conducted in triplicate, and the results are presented as the means ± SEMs. The differences between the results were assessed via one-way ANOVA and subsequently analyzed via post hoc Tukey's multiple comparisons and chi-square tests. GraphPad Prism version 9.5.1 software was used for statistical analysis. p values < 0.05 were considered statistically significant.

RESULTS AND DISCUSSION

Anti-inflammatory activity of the essential oil

The essential oil of *R. officinalis* was able to inhibit protein denaturation in a concentration-dependent manner, a commonly used indicator of anti-inflammatory potential. The anti-inflammatory activity of the oil is given in Figure 2. Inhibition of protein denaturation ranges between 3.07 ± 0.296% and 32.46 ± 2.229% at 25-200 µg/ml concentrations, respectively ($p<0.05$). The major phytochemicals in the essential oil, 1,8-cineole, α-pinene, and camphor, as mentioned in the literature may contribute the anti-inflammatory activity of the oil. 1,8-cineole has been shown to suppress pro-inflammatory cytokine production and reduce oxidative stress and α-pinene exhibits membrane-stabilizing (Iqbal et al. 2024; Salehi et al. 2019). The combined action of these phytochemicals contributes to the synergistic effect observed in the protein denaturation inhibition assay. Therefore, the essential oil showed significant and dose-dependent protective effects against heat-induced protein denaturation, supporting its potential as a natural anti-inflammatory agent. According to the results, rosemary essential oil can be considered a promising candidate for further pharmacological evaluation. These

findings align with the growing interest in plant-derived natural compounds as alternatives to synthetic anti-inflammatory drugs in the pharmaceutical industry.

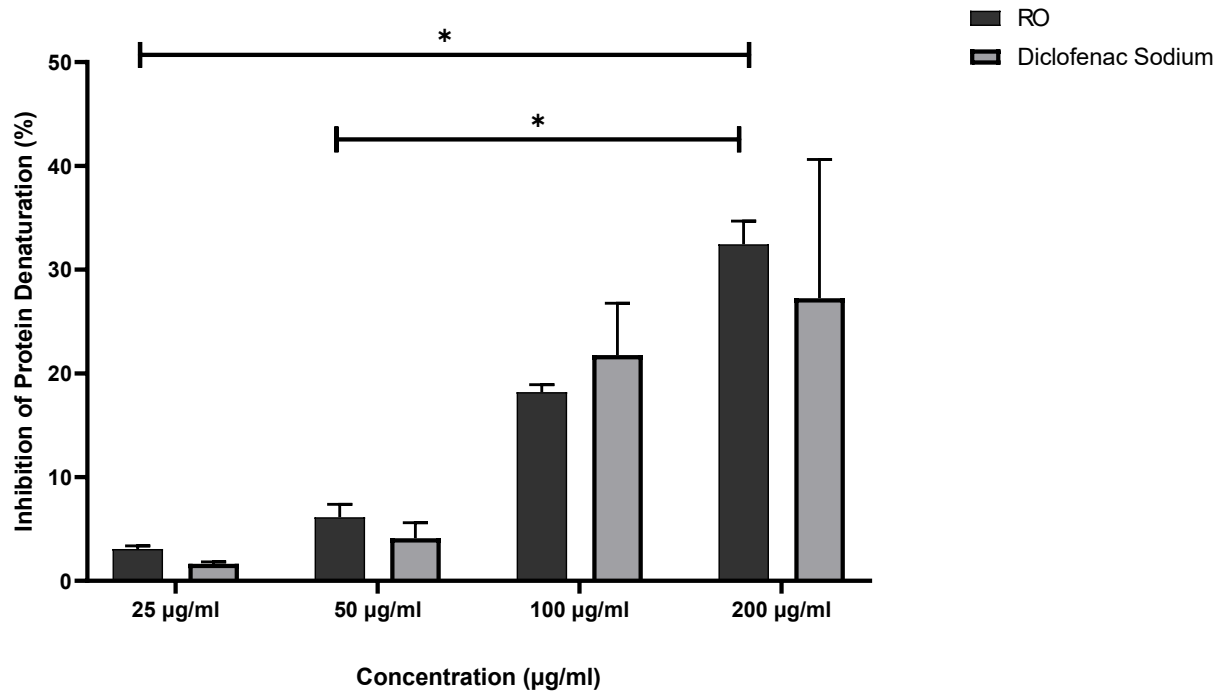

Figure 2: Anti-inflammatory activity of *R. officinalis* essential oil and diclofenac sodium. Percentage inhibition of *R. officinalis* essential oil and diclofenac sodium in protein denaturation inhibition assay. The results are presented as mean ± SEM (n=3); one-way ANOVA test, *P<0.05. RO: *Rosmarinus officinalis.*

Antibacterial activity of the essential oil and hydrosol

The results of the antibacterial activity testing were represented in Figure 3. The zones of inhibition of essential oil and hydrosol were detected as 13.6 ± 1.154 mm and 16.6 ± 1.527 mm, respectively. These data indicated moderate to strong anti-MRSA activity. One of the known gallic acid was used as a control, and its zone of inhibition was measured as 23.5 ± 1.527 mm. The zone produced by gallic acid against MRSA was significantly higher than those of the essential oil and hydrosol of *R. officinalis*, with p-values of 0.02 for hydrosol vs. gallic acid and 0.0003 for essential oil vs. gallic acid.

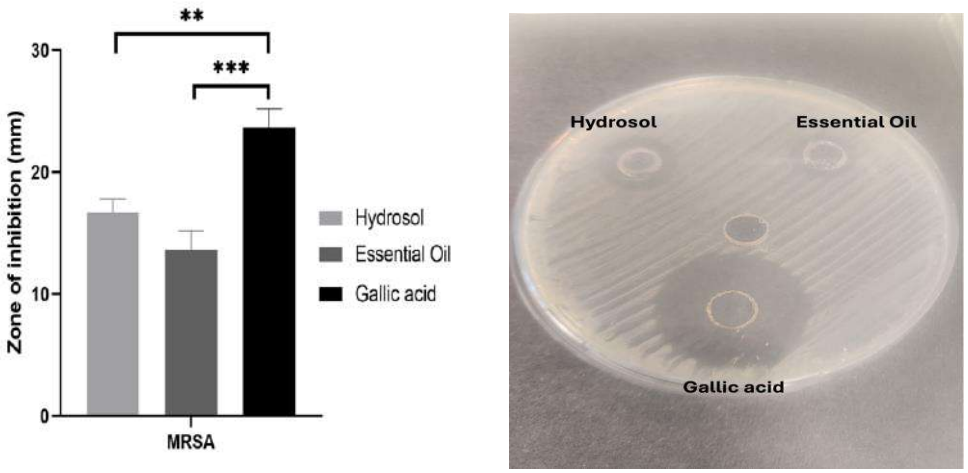

Figure 3: Zone of inhibition values of *Rosmarinus officinalis* hydrosol and essential oil against Methicillin-resistant *Staphylococcus aureus* (MRSA). The values are presented in millimeters (mm). A Chi-square test was conducted for statistical analysis, and a p-value of < 0.05 was considered statistically significant. The p-values for comparisons are as follows: hydrosol vs. gallic acid = 0.02, and essential oil vs. gallic acid = 0.0003.

As seen in Figure 3, the antibacterial activity of the hydrosol was found to be higher than that of the essential oil according to well diffusion method. Such a difference can be due to the fact that hydrosol contains water-soluble active components that diffuse more easily on water-based agar than those in the oil which are generally water insoluble.

The essential oil and hydrosol exerted a good anti-MRSA activity which was attributed to the presence of several active compounds such as 1,8-cineole, α-pinene, camphene and camphor. More precisely, in a previous research, the key active components detected in the essential oil of *Rosmarinus officinalis* L. were reported to be 1,8-cineole and camphor, which are all known to have strong antibacterial activity (Zaouali et al. 2010). Zaouali et al. (2010) showed that the oil of *R. officinalis* L. had a good range of antibacterial activity against a wide range of pathogens, both Gram-positive and Gram-negative, including *S. aureus*, similar to our study (Zaouali et al., 2010). In another study, the two key ingredients identified in the hydrosol were 1,8-cineole and borneol, which are known to exert a good antibacterial activity. Parallel to the finding of the present study, Gaspar-Pintiliescu et al. (2020) also reported antibacterial activity of *Rosmarinus officinalis* hydrosol against *S. aureus*.

In the previous research, the extracts of *R. officinalis* have been shown to exhibit antibacterial activity against MRSA similar to our study, as well as antibiofilm activity (Nakagawa et al. 2020). The active ingredients in *R. officinalis*, particularly carnosic acid and carnosol, have been shown to act as specific inhibitors of *S. aureus* RNAIII and psmα gene expression. Furthermore, as having antibacterial

activity De Oliveira et al. suggested the use of *R. officinalis* in toothpaste and soaps due to its antimicrobial properties (De Oliveira et al. 2017).

CONCLUSION

Rosmarinus officinalis essential oil was demonstrated to have anti-inflammatory and antibacterial activity against MRSA. The active ingredients, such as 1,8-cineole, α-pinene, camphene and camphor may contribute to these activities. These products may serve as a complementary and natural alternative to current medicines.

ACKNOWLEDGEMENT

The plant sample was collected from the aromatic garden of the KKTC Girişimci Kadınlar Derneği (GİKAD). We would like to thank the President of the Association, Dr. İçim Çağıner Kavuklu, for her support.

REFERENCES

An N, Van Hai LHL, Luong VH, Vinh NTH, Hoa PQ, et al. (2024). Antimicrobial Resistance Patterns of Staphylococcus Aureus Isolated at a General Hospital in Vietnam Between 2014 and 2021. Infection and Drug Resistance 17(January): 259–273.

Annemer S, Farah A, Stambouli H, Assouguem A, Almutairi MH, et al. (2022). Chemometric Investigation and Antimicrobial Activity of Salvia rosmarinus Spenn Essential Oils. Molecules 27(9): 2914.

Bhat P, Upadhya V, Hegde GR, Hegde HV, Roy S (2022). Attenuation of dermal wounds through topical application of ointment containing phenol enriched fraction of Caesalpinia mimosoides Lam. Frontiers in Pharmacology 13 1025848.

Couto RO, Conceicao EC, Chaul LT, Oliveira EMS, Martins FS, et al. (2012). Spraydried rosemary extracts: Physicochemical and antioxidant properties. Food Chem 131: 99–105.

De Oliveira JR, de Jesus D, Figueira LW, de Oliveira FE, Pacheco Soares C, et al. (2017). Biological activities of Rosmarinus officinalis L.(rosemary) extract as analyzed in microorganisms and cells. Experimental Biology and Medicine 242(6): 625–634.

El Aila NA, Al Laham NA, Ayesh BM (2017). Nasal carriage of methicillin resistant Staphylococcus aureus among health care workers at Al Shifa hospital in Gaza Strip. BMC Infectious Diseases 17(1): 1–7.

Hand R, Hadjikyriakou GN, Christodoulou CS (2011). No Title. Flora of Cyprus – a Dynamic Checklist.

Iqbal U, Malik A, Sial NT, Uttra AM, Rehman MFU, et al. (2024). Molecular insights of Eucalyptol (1,8-Cineole) as an anti-arthritic agent: in vivo and in silico analysis of IL-17, IL-10, NF-κB, 5-LOX and COX-2. Inflammopharmacology 32(3): 1941–1959.

Kabotso DEK, Neglo D, Gaba SE, Danyo EK, Dayie AD, et al. (2024). In Vitro Evaluation of Rosemary Essential Oil: GC-MS Profiling, Antibacterial Synergy, and Biofilm Inhibition. Pharmaceuticals, 17(12): 1653.

Kim MW, Greenfield BK, Snyder RE, Steinmaus CM, Riley LW (2018). The association between community-associated Staphylococcus aureus colonization and disease: a meta-analysis. BMC Infectious Diseases 18(1): 86.

Nakagawa S, Hillebrand GG, Nunez G (2020). antibiotics Rosmarinus o ffi cinalis L . (Rosemary) Extracts Containing Carnosic Acid and Carnosol are Potent Quorum Sensing Inhibitors of Staphylococcus aureus Virulence.

Salehi B, Upadhyay S, Erdogan I, Kumar A, Jayaweera S, et al. (2019). Therapeutic Potential of α- and β-Pinene: A Miracle Gift of Nature. Biomolecules 9(11): 738.

Talib A, Sa'ady A, Al-Sa'ady AT (2020). Antibacterial screening for five local medicinal plants against nosocomial pathogens: Klebsiella pneumoniae and Staphylococcus epidermidis. EurAsian Journal of BioSciences Eurasia J Biosci 14: 553–559.

Zaouali Y, Bouzaine T, Boussaid M (2010). Essential oils composition in two Rosmarinus officinalis L. varieties and incidence for antimicrobial and antioxidant activities. Food and Chemical Toxicology 48(11): 3144–3152.

Research Article EMUJPharmSci ISSN 2651-3587 https://dergipark.org.tr/emujpharmsci

EMU Journal of Pharmaceutical Sciences

EMUJPharmSci

Synthesis of *N*'-(diphenylmethylene)-3-(amino)propanehydrazide Derivatives and Evaluation for Cholinesterase Inhibitor and Antioxidant Activities

S. Berfin Gungor[1], Burcu Kilic[1*], Deniz S. Dogruer[1]

[1]Gazi University, Department of Pharmaceutical Chemistry, Faculty of Pharmacy, Ankara, Türkiye.

Abstract

Alzheimer's disease (AD) is a progressive neurodegenerative disorder and the most prevalent form of dementia, affecting millions of individuals worldwide. It is characterized by a gradual decline in cognitive function, ultimately impairing patients' ability to perform daily activities. Multiple pathogenic mechanisms have been implicated in AD, including disturbances in the cholinergic system, oxidative stress, metal ion dysregulation, and amyloid-β (Aβ) aggregation.

In the present study, four novel *N*'-(diphenylmethylene)-3-(amino)propanehydrazide derivatives were designed, synthesized, and subsequently evaluated for their cholinesterase inhibitory and antioxidant activities. These compounds may serve as promising starting points for the development of new molecular design strategies targeting AD-related pathways.

Keywords

Alzheimer's disease, antioxidant activity, cholinesterase inhibition.

Article History

Submitted: 02 December 2025 Accepted: 17 December 2025 Published Online: December 2025

Article Info

***Corresponding author:** Burcu Kilic **email:** burcukahya@gazi.edu.tr

Research Article:
Volume: 8 Issue: 3 Pages: 132-140
DOI: 10.54994/emujpharmsci.1834518

INTRODUCTION

Alzheimer's disease (AD) is a progressive neurodegenerative disorder characterized by brain damage affecting thought, memory, and behavior (Feng and Wang 2012). This damage leads to dementia, which impairs an individual's ability to perform daily activities (Feng and Wang, 2012). The disease typically begins with memory loss and progresses to other cognitive impairments such as confusion, difficulty in decision-making, speech and language problems, and changes in personality and behavior (Breijyeh and Karaman, 2020). The exact cause of the disease remains unknown (Passeri et al. 2022); however, various factors, including genetic and lifestyle-related influences, are believed to contribute to its development. Current treatments for AD are primarily symptomatic, aiming to slow the decline in cognitive symptoms and manage the behavioral and psychological symptoms associated with dementia (Passeri et al. 2022). Some key factors thought to play an important role in the pathogenesis of AD include: Cholinesterase enzymes are responsible for the hydrolysis of acetylcholine (ACh) (Chen et al. 2022). In AD, there is a significant decrease in ACh levels in the brain. This decrease in ACh level results from the loss of cholinergic neurons and an increase in the activity of cholinesterase enzymes. Cholinesterase inhibitors (ChEIs) constitute an important class of drugs used in the treatment of AD, such as donepezil, rivastigmine, and galantamine (Marucci et al. 2021). They support cognitive functions by inhibiting the enzyme responsible for the degradation of ACh. Unfortunately, these ChEIs only alleviate the symptoms of Alzheimer's disease and do not modify the underlying pathology. As a result, there remains an urgent and ongoing need for the development of novel therapeutic agents.

Amyloid-β (Aβ), which is formed by the proteolytic cleavage of amyloid precursor protein (APP), accumulates in the brain in AD and forms amyloid plaques (Passeri et al. 2022). These plaques disrupt synaptic transmission, leading to neurotoxicity.

In AD, the tau protein becomes hyperphosphorylated and aggregates within neurons, forming neurofibrillary tangles (NFTs). These NFTs impair neuronal function and lead to neurodegeneration (Feng and Wang, 2012). An imbalance between reactive oxygen species (ROS) and the antioxidant defense system leads to cellular damage and is highly implicated in AD pathogenesis (Feng and Wang, 2012). Metal ion dyshomeostasis in the brain can promote the aggregation and deposition of Aβ and tau proteins, thereby exacerbating AD pathogenesis (Chen et al. 2023). While AD pathology, amyloid plaques, and NFTs

induce the activation of microglia and astrocytes, leading to the release of pro-inflammatory cytokines and resulting in progressive neuroinflammation (Breijyeh and Karaman, 2020).

The objective of this study was the synthesis of *N*'-(diphenylmethylene)-3-(amino) propanehydrazide derivatives and the in vitro evaluation of their cholinesterase inhibitory and antioxidant properties.

The synthesis was carried out in three steps (Figure 1). In the first step, intermediate 1 (Int-1) was obtained from the condensation of benzophenone with hydrazine. Following, the nucleophilic substitution of Int-1 with chloropropionyl chloride yielded intermediate 2 (Int-2). Finally, various tertiary amine derivatives were reacted with Int-2 in order to obtain the final compounds (Compound 1-4).

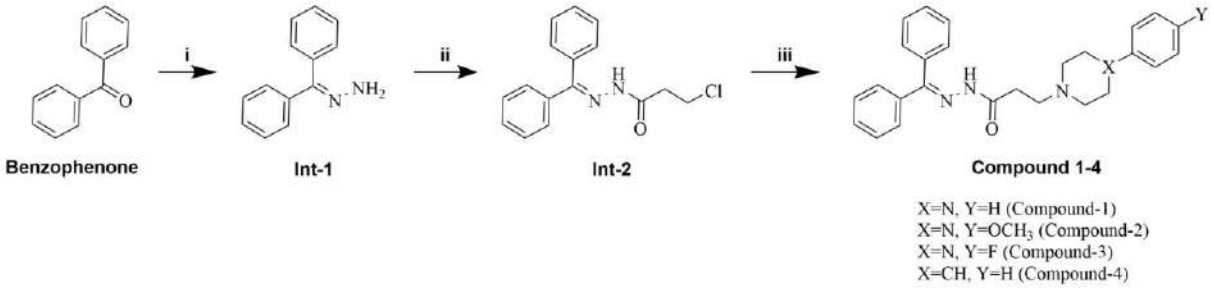

Figure 1: Synthesis of *N'*-(diphenylmethylene)-3-(amino)propanehydrazide derivatives **(1-4)**. Reagents and conditions: **(i)** Hydrazine monohydrate, acetic acid, EtOH, reflux, 3 h; **(ii)** Chloropropionyl chloride, pyridine, DCM, rt, 0.5 h; (iii) Tertiary amine derivative, DMF, rt, 4 h.

MATERIALS AND METHODS

Chemical studies

All chemicals and solvents were acquired from commercial suppliers (Sigma Aldrich, Merck, Isolab). Merck 60 F_{254} plates were used for TLC. Schmelzpunkt SMP-II digital apparatus was used for melting point (mp) detection. NMR spectra were recorded using a Bruker Avance Neo 500MHz FT-NMR spectrometer. Waters LCT Premier XE Mass Spectrometer operating in electrospray ionization (ESI) mode was recruited to collect HRMS. The mass spectrometer was also coupled to an AQUITY Ultra Performance Liquid Chromatography system with UV detector monitoring at 254 nm.

Diphenylmethylene hydrazine (Int-1) (CAS No: 5350-57-2)

To a flask containing a solution of 1.0 g (5.49 mmol, 1 eq) of benzophenone in 20 mL of ethanol, 0.2 mL (3.29 mmol, 0.6 eq) of acetic acid and 2 mL (27.45 mmol, 5 eq) of hydrazine monohydrate were subsequently added. The resulting mixture was refluxed while stirring for 3 hours. At the end of this period solvent was

evaporated under reduced pressure using a rotary evaporator to yield the crude solid product (Int-1). The crude Int-1 was dissolved in a minimum amount of ethyl acetate and hexane, and the solution was partially concentrated by heating and allowed to stand at room temperature for precipitation. The precipitated Int-1 was collected by filtration and washed with a mixture of diethyl ether and petroleum ether. White crystals. Yield: 874 mg, 81%. mp: 98°C (95-98°C in literature). HRMS (ESI) $[M+H]^+$ m/z for $C_{13}H_{13}N_2$ calculated: 197.1079, found: 197.1078.

3-Chloro-*N*'-(diphenylmethylene) propanhydrazide (Int-2) (CAS No: 79289-21-7)

In a flask, 0.874 g (4.45 mmol, 1 eq) of Int-1 was dissolved in 5 mL of DCM. Subsequently, 0.359 mL (4.45 mmol, 1 eq) of pyridine was introduced. The reaction mixture was then stirred at room temperature. To this mixture, 0.425 mL (4.45 mmol, 1 eq) of chloropropionyl chloride was added dropwise, and the reaction was allowed to stir for 30 minutes. Upon completion, the DCM was evaporated under reduced pressure using a rotary evaporator, yielding the crude Int-2. The remaining crude solid was triturated with water, and the solid was collected by filtration. The precipitated Int-2 was collected by filtration and washed with a mixture of diethyl ether and petroleum ether. White crystals. Yield: 890 mg, 71%. mp: 136°C (130-131 °C in literature). HRMS (ESI) $[M+H]^+$ m/z for $C_{16}H_{16}ClN_2O$ calculated: 287.0951, found: 287.0963.

General Procedure for the Synthesis of Final Compounds (Compound 1–4)

0.5 g (1.748 mmol, 1 eq) of Int-2 was added to a flask and dissolved in 4 mL of DMF. Then, 2.0 eq of the corresponding tertiary amine derivative was added, and the mixture was stirred. The reactions were complete in 4 hours. Upon completion, water was added to the reaction mixture, and the resulting cloudy mixture was transferred into a beaker. To induce precipitation of the product, the beaker was heated while stirring for a short period. The precipitated crude product was filtered off and crystallized with the appropriate solvent.

N'-(diphenylmethylene)-3-(4-phenylpiperazin-1-yl)propanehydrazide (Compound-1)

Following the general method, 0.5 g (1.748 mmol, 1 eq) Int-2 and 0.534 mL (3.496 mmol, 2 eq) 4-phenylpiperazine were stirred at rt for 4 h. Crystallization solvent: EtOH, White crystals. Yield: 210 mg, 29%. mp: 142°C. HRMS (ESI) $[M+H]^+$ m/z for $C_{26}H_{29}N_4O$ calculated: 413.2341, found: 413.2328. ^1H NMR (500 MHz, $CDCl_3$) δ 10.53, 8.42 (two s, 1H, NH/OH), 7.68 – 7.44 (m, 5H, ArH), 7.45 – 7.21 (m, with $CDCl_3$, 7H, ArH), 7.02 – 6.82 (m, 3H, ArH),

3.27 (t, *J* = 4.5 Hz, 3H), 3.16, 2.95 (two t, *J* = 7.2 Hz, 3H), 2.84 – 2.70 (m, 4H), 2.63 – 2.54 (m, 1H), 2.42 (t, *J* = 5.1 Hz, 1H). ^{13}C NMR (126 MHz, $CDCl_3$) δ 173.81, 168.80, 154.49, 151.28, 150.92, 150.56, 137.57, 136.92, 133.63, 131.53, 130.06, 130.00, 129.86, 129.77, 129.75, 129.63, 129.13, 129.10, 128.81, 128.45, 128.40, 128.19, 128.11, 127.38, 119.86, 119.77, 116.13, 116.02, 77.30, 77.05, 76.79, 58.43, 53.54, 53.37, 53.14, 52.50, 49.09, 48.13, 32.01, 30.54.

N′-(diphenylmethylene)-3-(4-(4-methoxyphenyl)piperazin-1-yl)propanehydrazide (Compound-2)

Following the general method, 0.5 g (1.748 mmol, 1 eq) Int-2 and 0.672 g (3.496 mmol, 2 eq) 1-(4-methoxyphenyl)piperazine were stirred at rt for 4 h. Crystallization solvent: Acetonitrile, White crystals. Yield: 283 mg, 37%. mp: 156°C. HRMS (ESI) $[M+H]^+$ m/z for $C_{27}H_{31}N_4O_2$ calculated: 443.2447, found: 443.2460. ^{1}H NMR (500 MHz, $CDCl_3$) δ 10.56, 8.41 (two s, 1H, NH/OH), 7.64 – 7.45 (m, 5H, ArH), 7.43 – 7.24 (m, with $CDCl_3$, 5H, ArH), 6.97 – 6.78 (m, 4H, ArH), 3.81, 3.79 (two s, 3H, OCH_3), 3.21 – 3.07 (m, 4.5H), 2.95 (t, *J* = 7.2 Hz, 1.5H, -$CH_2$$CH_2$C=O), 2.78 (bs, 3H), 2.65 (t, *J* = 4.6 Hz, 1H), 2.61 – 2.53 (m, 1H), 2.41 (t, *J* = 4.6 Hz, 1H). ^{13}C NMR (126 MHz, $CDCl_3$) δ 173.84, 168.84, 154.51, 153.86, 150.54, 145.68, 145.28, 137.59, 136.91, 133.64, 131.53, 130.04, 129.99, 129.86, 129.77, 129.74, 129.62, 128.84, 128.45, 128.40, 128.29, 128.20, 128.10, 127.38, 118.28, 118.10, 114.45, 114.39, 77.30, 77.25, 77.05, 76.80, 55.58, 53.52, 53.36, 53.23, 52.62, 50.57, 49.55, 31.98, 30.52.

N′-(diphenylmethylene)-3-(4-(4-fluorophenyl)piperazin-1-yl)propanehydrazide (Compound-3)

Following the general method, 0.5 g (1.748 mmol, 1 eq) Int-2 and 0.630 g (3.496 mmol, 2 eq) 1-(4-fluorophenyl)piperazine were stirred at rt for 4 h. Crystallization solvent: EtOH, White crystals. Yield: 365 mg, 49%. mp: 150°C. HRMS (ESI) $[M+H]^+$ m/z for $C_{26}H_{28}FN_4O$ calculated: 431.2247, found: 431.2237. ^{1}H NMR (500 MHz, $CDCl_3$) δ 10.50, 8.41 (s, 1H, NH/OH), 7.63 – 7.45 (m, 5H, ArH), 7.44 – 7.20 (m, with $CDCl_3$, 5H, ArH), 7.04 – 6.74 (m, 4H, ArH), 3.20 – 3.13 (m, 4.5H), 2.95 (t, *J* = 7.5 Hz, 1.5 H), 2.77 (bs, 3H), 2.67 (t, *J* = 5.0 Hz, 1H), 2.63 – 2.53 (m, 1H), 2.42 (t, *J* = 5.0 Hz, 1H). ^{13}C NMR (126 MHz, $CDCl_3$) δ 173.79, 168.77, 158.16, 156.26, 154.44, 150.57, 147.96, 147.57, 137.56, 136.91, 133.67, 131.51, 130.01, 129.87, 129.79, 129.75, 129.61, 128.85, 128.44, 128.40, 128.29, 128.19, 128.12, 127.38, 117.91, 117.85, 117.70, 117.63, 115.61, 115.44, 77.30, 77.25, 77.05, 76.79, 53.49, 53.35, 53.13, 52.50, 50.11, 49.07, 32.01, 30.55.

N′-(diphenylmethylene)-3-(4-phenylpiperidin-1-yl)propanehydrazide (Compound-4)

Following the general method, 0.5 g (1.748 mmol, 1 eq) Int-2 and 0.563 g (3.496 mmol, 2 eq) 4-phenylpiperidine were stirred at rt for 4 h. Crystallization solvent: Ether, White crystals. Yield: 243 mg, 34%. mp: 130°C. HRMS (ESI) $[M+H]^+$ m/z for $C_{27}H_{29}N_3O$ calculated: 412.2389, found: 412.2399. ^1H NMR (500 MHz, $CDCl_3$) δ 10.74, 8.41 (s, 1H, NH/OH), 7.66 – 6.90 (m, 15H, ArH), 3.27 – 3.10 (m, 3H), 2.93 (t, *J* = 7.6 Hz, 1H), 2.81, 1.64 (d, *J* = 12.4 Hz, 1H), 2.61 – 2.36 (m, 3H), 1.89 (bs, 3H), 1.14 (qd, *J* = 12.4, 3.3 Hz, 1H). ^{13}C NMR (126 MHz, $CDCl_3$) δ 174.06, 169.00, 154.64, 150.47, 146.28, 145.70, 137.69, 136.93, 133.65, 131.57, 130.00, 129.98, 129.85, 129.75, 129.71, 129.46, 128.86, 128.47, 128.45, 128.38, 128.36, 128.30, 128.10, 127.40, 126.90, 126.76, 126.24, 126.18, 77.31, 77.05, 76.80, 54.32, 53.86, 53.53, 53.38, 42.61, 42.03, 33.39, 32.29, 32.16, 30.74.

Cholinesterase Inhibition Assay

AChE (electric eel) and BChE (equine serum) from Sigma-Aldrich were employed in the assays. The % inhibitory activities of AChE and BChE for the test compounds at a 10 μM concentration were determined using the modified Ellman's method (Ellman et al. 1961), as previously reported (Bardakkaya et al. 2023; Kilic et al. 2023). The formation of the yellow color was measured at 412 nm using the SpectraMax ABS Plus ELISA Microplate Reader. Electric eel AChE (type-VI-S, EC 3.1.1.7) and equine serum BChE (EC 3.1.1.8), 5,5′-di 5,5′-di-thiobis-2-nitrobenzoic acid (DTNB), acetylthiocholine iodide (ATI), butyrylthiocholine iodide (BTI), and Tris were purchased from Sigma Aldrich. Donepezil and Galantamine were used as the reference drug at 10μM concentration. Sample compounds were dissolved in DMSO; the final reaction mixture contained 1% DMSO. At this concentration, DMSO has no inhibitory effect on both enzymes.

In vitro Antioxidant Activity Assay

DPPH radical scavenging activity was conducted using the UV methodology suggested by Blois (Blois, 1958). Primarily, the samples and the reference (i.e., gallic acid) were dissolved in ethanol to achieve a reaction concentration of 10 μM (i.e., 20 μL). These solutions were added to a 0.15 mM DPPH solution in ethanol (i.e., 180 μL). Following incubation at room temperature for 30 minutes, the unchanged DPPH amount was measured at 517 nm employing SpectraMax ABS Plus ELISA Microplate Reader. The percent DPPH radical scavenging activity was measured through the following formula: [(A control – A sample)/A control] × 100, wherein the A control is the result obtained in the absence of the test sample, and A sample is the result obtained in the presence of the test sample or the reference. Each assay was performed in triplicate, and the mean ± SD was calculated.

RESULTS AND DISCUSSION

Chemistry

Acylhydrazone scaffolds are known to exhibit several types of isomerism, including *E/Z* geometrical isomers around the C=N bond, cis/trans amide conformers around the C(O)–NH bond, rotational isomers around the N–N bond, as well as amide/iminol tautomers. Consequently, the acylhydrazone compounds displayed duplicated signal sets in their ^{1}H and ^{13}C NMR spectra. This phenomenon was also discussed in our previous study on *N*'-(quinolin-4-ylmethylene)propanehydrazide derivatives (Kilic and Dogruer, 2024). Similarly, compounds 1-4 exhibited split peak sets for specific proton and carbon atoms. Notably, the iminol proton resonated at approximately 10.5 ppm, while the amide proton appeared around 8.5 ppm, with an integration ratio of about 0.3:0.7, respectively. A comparable integration ratio was consistently observed across all duplicated signal sets.

Cholinesterase inhibition

The compounds were screened at concentrations of 10, 25, 50, and 100 µM to evaluate their ChE inhibitory potential, and the results are summarized in Table 1. None of the compounds exhibited inhibitory activity against AChE; however, they demonstrated measurable inhibition toward BChE. Interestingly, the compounds 3 and 4 showed higher BChE inhibition at 50 µM than at 100 µM, which is likely attributable to a solvation-related issue at higher concentrations. According to the 50 µM assay results, compound 4 (%78.9±2.3) was identified as the most effective compound in the series.

Table 1: Cholinesterase inhibition assay results (n.a.; no activity, n.t.; not tested).

	AChE inhibition %				**BuChE inhibition %**			
	10 µM	**25 µM**	**50 µM**	**100 µM**	**10 µM**	**25 µM**	**50 µM**	**100 µM**
Compound 1	n.a.	n.a.	n.a.	n.a.	%15.9±2.4	%29.7±4.5	%43.9±3.3	%58.4±3.8
Compound 2	n.a.	n.a.	n.a.	n.a.	%8.2±0.2	%18.0±2.6	%26.6±1.8	%40.1±3.5
Compound 3	n.a.	n.a.	n.a.	n.a.	%11.8±0.9	%28.5±2.2	%44.5±1.3	%35.1±6.0
Compound 4	n.a.	n.a.	n.a.	n.a.	%40.4±1.5	%54.9±6.2	%78.9±2.3	%65.8±4.2
Donepezil	%99.1±0.5	n.t.	n.t.	n.t.	%85.9±1.5	n.t.	n.t.	n.t.
Galantamin	%88.5±0.7	n.t.	n.t.	n.t.	%31.7±2.4	n.t.	n.t.	n.t.

Antioxidant activity

The compounds were evaluated for their radical scavenging activity using the DPPH assay, and the results are summarized in Table 2. Unfortunately, none of the compounds exhibited meaningful radical scavenging activity (≤5%) at concentrations of 10 or 50 µM. When the concentration was increased to 100 µM, a slight increase was observed for compounds 1 and 4; however, these increases remain insignificant and are not considered indicative of genuine antioxidant potential.

Table 2: DPPH assay results (n.a.; no activity).

	10 µM	50 µM	100 µM
Compound 1	n.a.	n.a.	% 6.7±0.3
Compound 2	n.a.	n.a.	n.a.
Compound 3	n.a.	n.a.	n.a.
Compound 4	n.a.	n.a.	% 9.8±0.8
Gallic acid	%38.9±1.3	%78.6±0.8	%92.4±0.5

CONCLUSION

In this study, four novel *N*'-(diphenylmethylene)-3-(amino) propanehydrazide derivatives were successfully designed, synthesized, and evaluated for their cholinesterase inhibitory and antioxidant properties. NMR analyses confirmed the presence of multiple isomeric forms, consistent with the known structural behavior of acylhydrazone-based compounds.

Biological evaluation revealed that none of the compounds exhibited activity toward AChE; however, all showed varying degrees of inhibition against BChE, with compound 4 identified as the most promising inhibitor. The DPPH assay showed that the derivatives lacked significant radical scavenging activity.

Overall, the findings indicate that this scaffold may serve as a useful starting point for designing new BChE-selective inhibitors, and further structural optimization could enhance their water solubility and pharmacological potential for applications related to AD.

ACKNOWLEDGMENTS

This study was supported by TUBITAK under grant 2209-A (2024-1, Project No: 1919B012420797).

REFERENCES

Bardakkaya M, Kilic B, Sagkan RI, Aksakal F, Shakila S, et al. (2023). Synthesis and evaluation of multitarget new 2-aminothiazole derivatives as potential anti-Alzheimer's agents. *Archiv der Pharmazie* **356**(8): 2300054.

Blois MS (1958). Antioxidant Determinations by the Use of a Stable Free Radical. *Nature* **181**(4617): 1199-1200.

Breijyeh Z, Karaman R (2020). Comprehensive Review on Alzheimer's Disease: Causes and Treatment. *Molecules* **25**(24).

Chen LL, Fan YG, Zhao LX, Zhang Q, Wang ZY (2023). The metal ion hypothesis of Alzheimer's disease and the anti-neuroinflammatory effect of metal chelators. *Bioorg Chem* **131:** 106301.

Chen ZR, Huang JB, Yang SL, Hong FF (2022). Role of Cholinergic Signaling in Alzheimer's Disease. *Molecules* **27**(6).

Ellman GL, Courtney KD, Andres VJ, Feather-Stone RM (1961). A New and Rapid Colorimetric Determination of Acetylcholinesterase Activity. *Biochemical Pharmacology* **7**: 88-95.

Feng Y, Wang X (2012). Antioxidant therapies for Alzheimer's disease. *Oxid Med Cell Longev* 472932.

Kilic B, Bardakkaya M, Ilıkcı Sagkan R, Aksakal F, Shakila S, et al. (2023). New thiourea and benzamide derivatives of 2-aminothiazole as multi-target agents against Alzheimer's disease: Design, synthesis, and biological evaluation. *Bioorganic Chemistry* **131**: 106322.

Kilic B, Dogruer DS (2024). Synthesis and investigation of the cholinesterase inhibitory and antioxidant capacities of some novel N'-(quinolin-4-ylmethylene)propanehydrazides against Alzheimer's disease. *Drug Development Research* **85**(3): e22183.

Passeri E, Elkhoury K, Morsink M, Broersen K, Linder M, et al. (2022). Alzheimer's Disease: Treatment Strategies and Their Limitations. *Int J Mol Sci* **23**(22).

Research Article EMUJPharmSci ISSN 2651-3587 https://dergipark.org.tr/emujpharmsci

EMU Journal of Pharmaceutical Sciences

EMUJPharmSci

Development and Validation of a New RP-HPLC Method for Simultaneous Estimation of Butenafine Hydrochloride and Curcumin in Bulk and Pharmaceutical Dosage Form

E. Vildan Burgaz [1]*, Leyla Beba Pozharani[1]

[1]Eastern Mediterranean University, Faculty of Pharmacy, Famagusta, North Cyprus via Mersin 10, Türkiye.

Abstract

A new, simple and sensitive reversed-phase high-performance liquid chromatographic (RP-HPLC) method was developed and validated for the simultaneous quantitative determination of Butenafine hydrochloride (BUT) and Curcumin (CUR) in bulk and combined pharmaceutical dosage form. This method is required for routine quality control of emerging topical formulations containing this antifungal–anti-inflammatory combination. Chromatographic separation was achieved on a C18 column (250 × 4.6 mm, 5 µm) column using a mobile phase consisting of Methanol: Water (90:10 v/v) at a flow rate of 1.0 mL/min with isocratic elution. Detection was performed at 254 nm. The method was validated in accordance with ICH guidelines for specificity, linearity, accuracy, precision, limits of detection (LOD) and limit of quantitation (LOQ), robustness and solution stability. Well-resolved peaks of BUT and CUR were obtained, with retention times of approximately 10.5 min and 1.8 min, respectively. The method showed excellent linearity over the concentration ranges of 5-15 µg/mL for BUT and CUR with correlation coefficients (r^2=0,9967 and r^2= 0,9976). Mean recoveries were within 98–102 % for both analytes, and intra- and inter-day precision values were below 2% RSD. The calculated LODs and LOQs indicated high sensitivity, and no interference from formulation excipients was observed. The proposed RP-HPLC method is simple, rapid, specific, accurate and precise, and is suitable for routine quality control analysis of BUT and CUR in bulk materials and combined pharmaceutical dosage forms.

Keywords

Butenafine hydrochloride, curcumin, ICH, method development, RP-HPLC, validation.

Article History

Submitted: 05 December 2025 Accepted: 18 December 2025 Published Online: December 2025

Article Info

***Corresponding author:** E. Vildan Burgaz **email:** vildan.burgaz@emu.edu.tr

Research Article:
Volume: 8 Issue: 3 Pages: 141-152
DOI: 10.54994/emujpharmsci.1836844

INTRODUCTION

Superficial mycotic infections are among the most frequent skin diseases worldwide, typically caused by dermatophytes such as *Trichophyton, Microsporum and Epidermophyton* species that colonize keratinized tissues (skin, hair and nails). More severe mucosal or systemic fungal infections, frequently due to *Candida, Aspergillus* or *Pneumocystis* spp., are associated with considerable morbidity and may become life-threatening when inadequately treated. Over recent decades, the growing problem of resistance to both antibacterial and antifungal agents has emerged as a major clinical and public-health concern. Classical antifungal classes polyenes, azoles and allylamines primarily disrupt ergosterol or its biosynthetic pathway, yet resistance can arise through multiple routes, including changes in drug targets, alterations in sterol biosynthesis, reduced intracellular drug accumulation and overexpression of target enzymes. In this setting, rational topical combination therapies that can enhance efficacy, shorten treatment duration and limit resistance development have gained particular relevance (Ankam et al. 2009).

Butenafine hydrochloride (BUT; n-4-tert-butyl-benzyl-N-methyl-1-naphthalenemethylamine hydrochloride) is a synthetic benzylamine antifungal structurally related to allylamines. Its principal mechanism of action is selective inhibition of fungal squalene epoxidase, blocking conversion of squalene to lanosterol, which in turn causes intracellular squalene accumulation and depletion of ergosterol in the fungal cell membrane. This mechanism confers mainly fungicidal activity against dermatophytes and provides a broad spectrum of activity against superficial fungi. Topically, BUT is widely used for the management of dermatophytosis such as tinea corporis, tinea cruris and tinea pedis, and clinical studies have reported equal or superior performance compared to terbinafine, a closely related allylamine. Because of extensive first-pass metabolism and very low oral bioavailability, BUT is formulated almost exclusively for topical use. It dissolves readily in common organic solvents (e.g., methanol, ethanol, chloroform) but exhibits only limited solubility in water, a property that must be addressed in both formulation design and analytical method development (Ansari et al. 2020; Mahdi et al. 2021).

Curcumin (CUR), also known as diferuloylmethane, is a naturally occurring polyphenolic compound primarily

extracted from the rhizomes of *Curcuma longa* (family Zingiberaceae). It exhibits a broad spectrum of biological activities, including antioxidant, anti-inflammatory, antibacterial, antifungal, antiviral, antidiabetic, and anticancer effects. In the context of fungal infections, curcumin has demonstrated notable efficacy against various pathogenic fungi such as *Candida albicans, Aspergillus spp., Cryptococcus neoformans*, and *Paracoccidioides brasiliensis* (Forms, 2022).

Mechanistically, CUR exerts antifungal activity by inducing oxidative stress, inhibiting hyphal development through disruption of thymidine uptake, and interfering with key cellular processes such as ergosterol biosynthesis, membrane ATPase activity, and proteinase secretion. Notably, curcumin has also been identified as a modulator of multidrug resistance (MDR) in yeast strains like Saccharomyces cerevisiae, enhancing fungal susceptibility to conventional antifungal agents (Khwaza and Aderibigbe, 2023).

Co-formulating BUT and CUR in a single topical dosage form represents a rational therapeutic strategy. BUT provides targeted fungicidal activity via squalene epoxidase inhibition, while CUR offers complementary anti-inflammatory, antioxidant and additional antifungal effects. This multimodal approach has the potential to accelerate symptom relief, improve overall treatment outcomes and reduce the duration of therapy, which may in turn lower the risk of resistance associated with long-term monotherapy. Successful development of such fixed-dose combinations, however, depends on the availability of a sensitive, selective and efficient analytical procedure capable of simultaneously quantifying both active pharmaceutical ingredients in bulk materials and finished formulations (Dong et al. 2021; Ogidi et al. 2021; Pozharani et al. 2023).

Accordingly, the present study focuses on the development and validation of a new reversed-phase high-performance liquid chromatographic (RP-HPLC) method for the simultaneous determination of BUT and CUR in topical products. A rapid, stability-indicating method is essential not only for routine quality control, but also for formulation optimization, compatibility testing and solution stability studies of this promising combination therapy.

MATERIAL AND METHODS

Materials

Butenafine hydrochloride was kindly supplied by Berko Pharmaceuticals [Türkiye] as a gift sample. Curcumin and Carbopol 934P was obtained from Merck [Germany]. HPLC-grade methanol and

other solvents were purchased from Sigma-Aldrich. Double distilled water has been used for all experiments.

Preparation of the Hydrogel Formulation

Carbopol-based hydrogels containing BUT and CUR were prepared with cold method. Distilled water was cooled to ~4 °C in an ice bath, and Carbopol 934P (0.1% w/w) was slowly dispersed as the gelling agent under continuous stirring. The dispersion was kept at 4 °C for 24 h to ensure complete hydration and removal of air bubbles, then neutralized with triethanolamine to obtain a clear gel base. BUT and CUR were accurately weighed and incorporated into the Carbopol 934P hydrogel under gentle stirring, to obtain formulations containing 10 mg BUT and 10 mg CUR in each 1 g of hydrogel (Patel et al. 2009).

Instrumentation and Chromatographic Conditions

HPLC analysis was performed on a The Agilent 1260 Infinity HPLC system equipped with a quaternary pump, autosampler, column oven and UV–Vis detector. Data acquisition and processing were carried out using Agilent Chem Station software.

Chromatographic separation was achieved on a C18 column (250 × 4.6 mm, 5 µm) maintained at 25 °C. The mobile phase consisted of Methanol: Water (90:10 v/v), filtered through a 0.45 µm membrane filter and degassed by sonication prior to use. The flow rate was set at 1 mL/min with isocratic elution, and the injection volume was 10 µL. Detection was carried out at 254 nm, which provided adequate sensitivity for both analytes. The run time for each analysis was 15 min.

Analytical Method Validation

The developed RP-HPLC method was validated in accordance with ICH Q2(R1) guidelines. Validation parameters included specificity, linearity and range, accuracy, precision, limits of detection and quantitation (LOD and LOQ), and solution stability.

Preparation of Standard Solutions

A stock solution of BUT and CUR was prepared by accurately weighing 10.0 mg of BUT and 10.0 mg of CUR dissolving it in a small volume of mobile phase in a 25 mL volumetric flask, then diluting to volume with mobile phase.

125 µl from stock solution of BUT and CUR were transferred into 5 mL volumetric flask and diluted up to 5 mL with the mobile phase. For construction of calibration curves, a series of standard solutions were obtained covering the concentration range of 5–15 µg/mL for BUT and CUR. Each concentration level was injected in triplicate, and mean peak areas were plotted against concentration to generate the calibration curves.

Preparation of Sample Solutions

For assay of the pharmaceutical dosage form, an accurately weighed amount of product equivalent to 10 mg of BUT and 10 mg of CUR was transferred into a 10 mL volumetric flask. An appropriate volume of mobile phase was added, and the mixture was sonicated for 20 min to ensure complete extraction of the drugs. After cooling, the volume was adjusted to the mark with mobile phase and 100 µl from stock solution of BUT and CUR were transferred into 5 mL volumetric flask and diluted up to 5 mL with the mobile phase the solution was filtered through a 0.45 µm membrane filter.

Specificity

Specificity was assessed by analyzing chromatograms of blank, plain gel formulation, individual standard solutions of BUT and CUR. The method was considered specific if no interfering peaks were observed at the retention times corresponding to BUT and CUR.

Accuracy

Accuracy of the analytical method was determined by comparing the actual results with theoretical amounts. The recovery studies were evaluated in triplicate using three different concentrations (8 µg/ml, 10 µg/ml and 12 µg/ml) of both BUT and CUR.

Precision

Precision, defined as the closeness of agreement between repeated measurements, was assessed in terms of repeatability and intermediate precision. For repeatability (within-day precision), six independently prepared solutions of BUT and CUR (10 µg/mL each) were injected into the HPLC system under identical conditions. Intermediate precision (between-day precision) was evaluated by performing six consecutive injections of 10 µg/mL BUT and CUR solutions on two different days. For both analyses, the standard deviation (SD) and relative standard deviation (RSD) of the peak areas were calculated to characterize method precision.

Linearity and Range

Linearity was established by analyzing calibration standards over the ranges of 5–15 µg/mL for BUT and CUR. Each concentration was injected in triplicate and mean peak areas were used for linear regression analysis. The slope, intercept and correlation coefficient (r^2) were calculated for both analytes, and visual inspection of residuals was used to confirm linear behavior within the studied range.

Limits of Detection (LOD) and Limits of Quantitation (LOQ)

LOD and LOQ for BUT and CUR were estimated from calibration data using the

standard deviation (SD) of the response and the slope (S) of the calibration curve according to the equations:

LOD = 3.3 × (SD / S)

LOQ = 10 × (SD / S)

The calculated LOD and LOQ values reflected the sensitivity of the proposed method.

Robustness

Robustness was investigated by introducing small deliberate variations in chromatographic conditions, such as flow rate ±0.1 mL/min. The influence of these changes on system suitability parameters and assay results was evaluated.

Assay of Hydrogel Formulation

Drug content of BUT and CUR in the Carbopol 934P hydrogel was determined by dissolving an accurately weighed quantity of hydrogel (500 mg) in methanol. The dispersion was transferred into a 50 mL volumetric flask, sonicated for 20 min to ensure complete extraction of the APIs, and the volume was made up with the mobile phase (methanol: distilled water, 90:10, v/v). The resulting solution (theoretically containing 10 µg/mL of BUT and 10 µg/mL of CUR) was filtered through a 0.45 µm membrane filter and analyzed by the developed HPLC method. Drug content (mg/g) was calculated from the corresponding calibration curve.

Solution Stability

Stability of standard and sample solutions was assessed by keeping solutions at room temperature and analyzing them at specified time intervals up to 0–36 h. Peak areas and retention times were compared with those of freshly prepared solutions, and percentage change and %RSD were calculated.

RESULTS AND DISCUSSION

Method development and optimization

As existing HPLC methods in the literature describes procedures generally quantify BUT and CUR separately rather than in combination, individual methods for each drug were first collated and adapted as the foundation for simultaneous assay development (Ahmed et al. 2021; Ankam et al. 2009; Barth et al. 2011). On this foundation, a series of chromatographic conditions was systematically investigated to establish a robust method for the concurrent determination of both analytes. Different mobile phase systems (Methanol: Distilled water, Ammonium acetate buffer: Acetonitrile, and Methanol: Acetonitrile) were evaluated under isocratic elution with respect to retention behavior, resolution, peak symmetry and overall

analysis time. Among these, Methanol: Distilled water (90:10, v/v) afforded superior resolution, peak shape and symmetry. Under the optimized conditions, CUR and BUT eluted at 1.80 and 10.5 min, respectively, with well-defined peaks and a short total run time, thereby enhancing analytical throughput. The use of only two solvents, a flow rate of 1.0 mL/min and isocratic elution further contributed to lower operational cost, methodological simplicity and prolonged column/system lifetime. The final HPLC conditions, retention times and symmetry factors are summarized in Table 1.

Table 1: Data for optimized HPLC method.

Parameters	
Mobile phase:	Methanol: Distilled Water (90:10, v/v)
Flow rate :	1 mL/min
Injection volume:	10 µL
Wavelength:	254 nm
Dilution solvent:	Mobile phase
Retention time for BUT:	10.5 min
Retention time for CUR:	1.8 min
Symmetry factor for BUT:	0.812
Symmetry factor for CUR:	0.795

Under these optimized conditions, both analytes exhibited good peak symmetry and theoretical plate counts, indicating efficient separation on the selected column (Gupta et al. 2024).

Specificity

Chromatograms of blank mobile phase and placebo solution showed no peaks at the retention times corresponding to BUT and CUR, indicating absence of interference from solvents or excipients. Individual standard and mixed standard chromatograms demonstrated well-separated peaks for the two analytes. Sample chromatograms confirmed that excipients present in the dosage form did not co-elute with either drug, supporting the specificity of the method (Figure 1) (Kumar and Nanda, 2011).

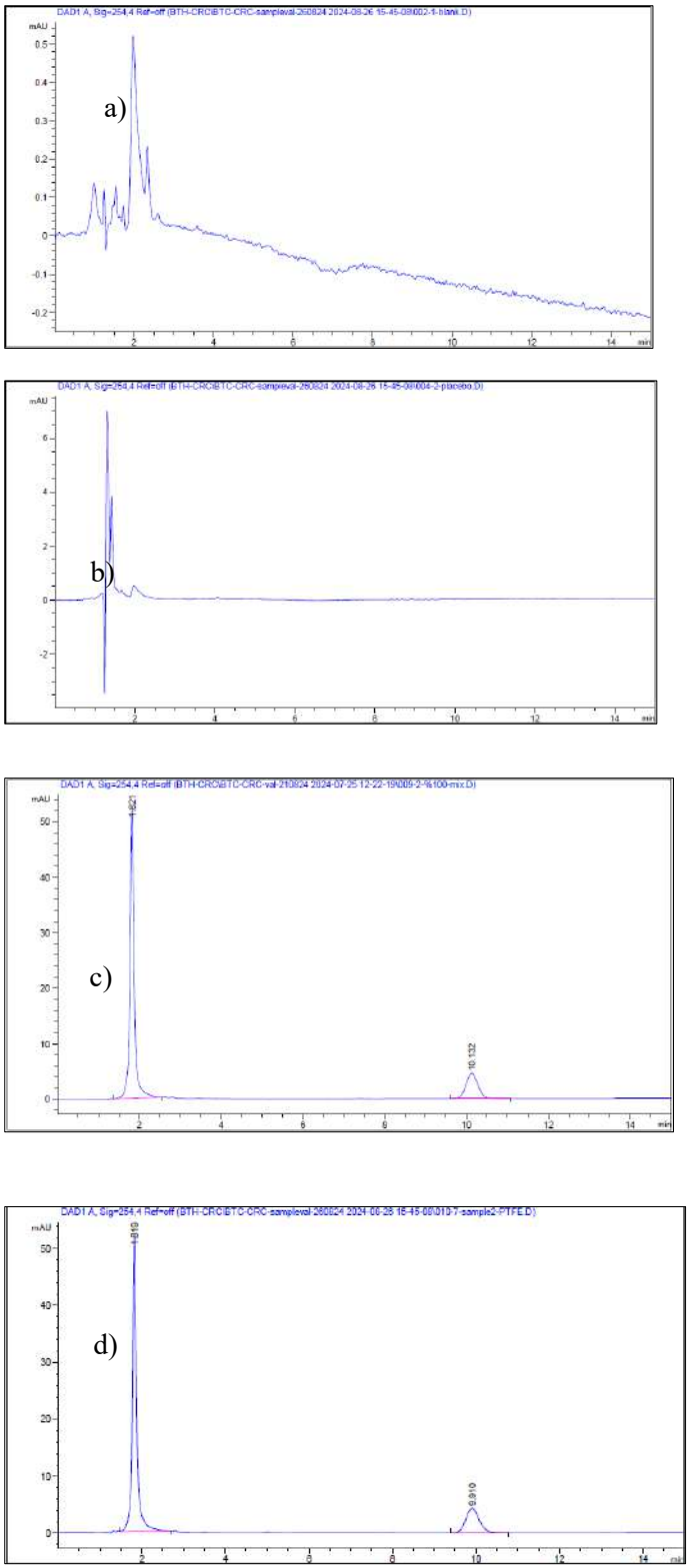

Figure 1: Chromatograms of (a) blank, (b) placebo (c) CUR and BUT injection (d) hydrogel formulation.

Linearity

Standard lines were plotted within 5-15 µg/ml concentration ranges, with the linear regression equation y = 9.3668x - 1.5311 (R^2 = 0.9967) and y = 38.666x + 2.752 (R^2 = 0.9976) for BUT and CUR, respectively. The calculated coefficients of determination for both BUT and CUR

were close to 1, and the low standard deviations confirmed that the instrument response was proportional to the analyte drug concentrations. The calibration analyses are presented in Figure 2 and Figure 3.

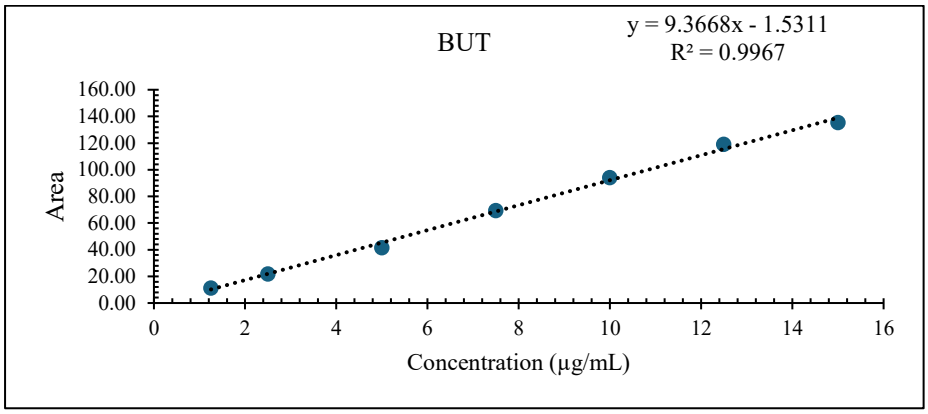

Figure 2: The regression line for BUT.

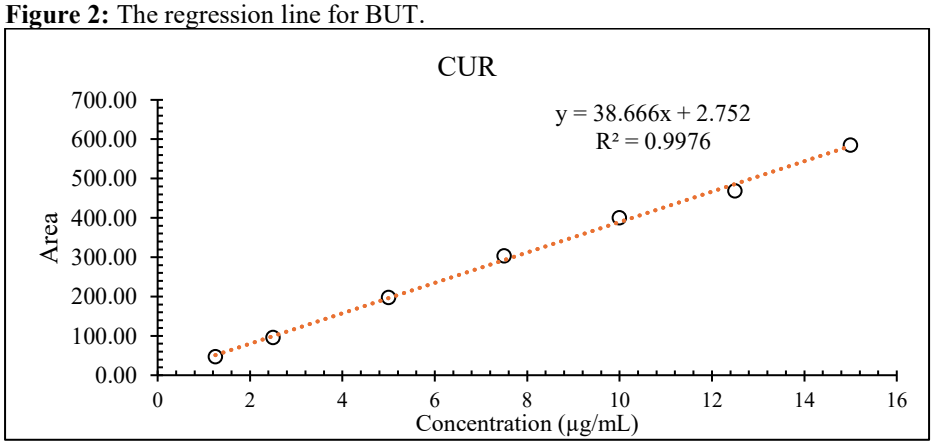

Figure 3: The regression line for CUR.

Accuracy

The accuracy of the analytical procedure was assessed using recovery studies. To this end, three concentration levels (80 %, 100 % and 120 %) were prepared from the stock solution containing BUT and CUR. The percentage recovery results for BUT and CUR are presented in Table 2 and Table 3, respectively. The relative deviations of the recovery percentages for both APIs were below 2%, demonstrating that the method meets the established accuracy criteria (Pozharani et al. 2022).

Table 2: Recovery results for BUT.

Theoretical cons. (µg/ml)	Practical cons. (µg/ml)	Recovery %	Theoretical cons. (µg/ml)	Practical cons. (µg/ml)	Recovery %	Theoretical cons. (µg/ml)	Practical cons. (µg/ml)	Recovery %
8	8.02	99.75	10	10.05	99.50	12	12.10	100.8
8	8.05	99.37	10	10.12	98.81	12	11.85	98.75
8	7.92	101.01	10	9.95	100.50	12	12.12	101.0
Mean		100.04			99.60			100.18
SD*		0.700			0.693			1.010
RSD%**		0.701			0.696			1.020

Table 3: Recovery results of CUR.

Theoretical cons. (µg/ml)	Practical cons. (µg/ml)	Recovery %	Theoretical cons. (µg/ml)	Practical cons. (µg/ml)	Recovery %	Theoretical cons. (µg/ml)	Practical cons. (µg/ml)	Recovery %
8	7.94	99.25	10	10.12	101.20	12	11.80	98.33
8	8.01	100.12	10	10.02	100.20	12	11.95	99.58
8	8.05	100.62	10	10.15	101.50	12	12.10	100.83
Mean		100.00			100.96			99.58
SD*		0.570			0.556			1.020
RSD%**		0.570			0.550			1.025

Precision

The precision of the method was evaluated through repeatability and intermediate precision studies. The repeatability and intermediate precision results are provided in Table 4.

The obtained repeatability RSD values were 1.45 % for BUT and 0.47 % for CUR. Intermediate precision was assessed through six analyses of each API performed in two consecutive days. All RSD values were below 2% across all assays, confirming that the method meets the established criteria for precision (Ibrahim et al. 2025).

Limits of detection and quantitation

To assess the sensitivity of the method, the LOD and LOQ values were calculated using the equation described above. The results presented in Table 5, indicate that the method is sufficiently sensitive for the determination of both BUT and CUR.

Table 4: Results for BUT and CUR, expressed as area mean and RSD, representing repeatability and intermediate precision.

BUT 10 µg/ml					**CUR 10 µg/ml**				
	1. Day		**2. Day**			**1. Day**		**2. Day**	
Sample	**Area**	**C (µg/ml)**	**Area**	**C (µg/ml)**	**Sample**	**Area**	**C (µg/ml)**	**Area**	**C (µg/ml)**
1	100.8	10.92	91.6	9.94	1	379.9	9.75	368.4	9.46
2	97.2	10.54	91.5	9.93	2	380.1	9.76	368.8	9.47
3	98.9	10.72	90.7	9.85	3	383.5	9.85	368.1	9.45
4	100.3	10.87	88.4	9.60	4	379.2	9.74	371.5	9.54
5	101.3	10.97	92.4	10.02	5	380.7	9.77	371.6	9.54
6	98.0	10.62	89.2	9.69	6	377.5	9.70	362.9	9.31
Mean	99.7	10.80	90.92	9.87	Mean	380.15	9.77	369.68	9.49
SD	1.48	0.15	1.37	0.14	SD	1.80	0.03	1.54	0.03
RSD %	1.45	1.46	1.50	1.48	RSD %	0.47	0.39	0.41	0.44

Table 5: Limits of detection (LOD) and quantitation (LOQ) for BUT and CUR.

	BUT (µg/ml)	**CUR (µg/ml)**
Limits of detection - LOD	0.60	0.45
Limits of quantitation - LOQ	1.98	1.48

Robustness

Deliberate variations in flow rate did not produce significant changes in retention times, peak areas or system suitability parameters. Assay results remained within acceptable limits and %RSD values were below [2%], indicating that the method is robust with respect to small operational fluctuations commonly encountered in routine laboratories.

Solution stability

Standard and sample solutions stored at room temperature for up to 0-36 h showed no significant changes in peak area or retention time compared with freshly prepared solutions. Percentage changes were below 2%, confirming that the analytes are stable in the selected solvent system over the time frame relevant for routine analysis (Bhujbal et al. 2024; Le et al. 2019).

Assay of The Hydrogel Formulation

The validated method was successfully applied to quantify the total drug content of BUT and CUR in the hydrogel formulation. The obtained results were consistent with the labeled amounts (Table 6).

Table 6: Assay of hydrogel formulation for combination of BUT and CUR.

	Theoretical Quantity (mg)	Assay (%)
BUT	10	99.75 (±0.52)
CUR	10	100.55 (±0.45)

CONCLUSION

A new reversed-phase HPLC method has been successfully developed and validated for the simultaneous determination of BUT and CUR in bulk and combined pharmaceutical dosage form. The method employs a conventional C18 column and an easily prepared mobile phase, offering sharp, well-resolved peaks with a short analysis time. Validation studies demonstrated that the method is specific, linear, accurate, precise, sensitive, robust and suitable for routine quality control.

Given its simplicity and performance characteristics, the proposed method can be readily implemented in quality control laboratories for the assay of existing and forthcoming Butenafine HCl–Curcumin combination products, and it may also support stability studies and formulation development.

ACKNOWLEDGMENTS

The authors declare no conflict of interest.

REFERENCES

Ahmed MM, Fatima F, Anwer MK, Ibnouf EO, Kalam MA, et al. (2021). Formulation and in vitro evaluation of topical nanosponge-based gel containing butenafine for the treatment of fungal skin infection. *Saudi J Medl* **29**(5): 467–477.

Ankam R, Mukkanti K, Durgaprasad S, Khan M (2009). *HPLC cream* 547–551.

Ansari MJ, Ahmed MM, Anwer MK, Aldawsari MF, Shahrani SMA, et al. (2020). Development and Validation of Simple, Rapid and Sensitive High- Performance Liquid Chromatographic Method for the Determination of Butenafine Hydrochloride. *J Pharm Res Int* **32**:116–125.

Barth AB, Pereira RL, de Vargas BA, Volpato NM (2011). A simple and rapid method to assess butenafine hydrochloride in skin samples and a comparative cutaneous retention study of two marketed formulations. *Biomedical Chromatography* **25**(10): 1132–1137.

Bhujbal S, Rupenthal ID, Agarwal P (2024). Development and validation of a stability-indicating HPLC method for assay of tonabersat in pharmaceutical formulations. *Methods* **231**(10): 178–185.

Dong HH, Wang YH, Peng XM, Zhou HY, Zhao F, et al. (2021). Synergistic antifungal effects of curcumin derivatives as fungal biofilm inhibitors with fluconazole. *Chemical Biology and Drug Design* **97**(5):1079–1088.

Forms, P. (2022). Curcumin : Biological Activities and Modern. *Antibiotics* **11**(2): 135.

Gupta P, Sharma S, Gupta A, Kawish SM, Iqbal M, et al. (2024). Development and Validation of a Robust RP-HPLC Method for the Simultaneous Analysis of Exemestane and Thymoquinone and Its Application to Lipid-Based Nanoformulations. *ACS Omega* **9**(28): 30120–30130.

Ibrahim AE, Farouk M, Alamir SG, Salman BI, Belal TS, et al. (2025). A quality-by-design optimized LC method for navigating degradation kinetics and quantification of favipiravir in the presence of degradation products and manufacturing impurities. *BMC Chemistry* **19**(1).

Khwaza V, Aderibigbe BA (2023). Antifungal Activities of Natural Products and Their Hybrid Molecules. *Pharmaceutics* **15**(12).

Kumar A, Nanda S (2011). A validated high performance liquid chromatographic method for estimation of bromhexine and terbutaline in bulk and tablet dosage forms. *Pharm Methods* **2**(4): 218–222.

Le THH, Phung TH, Le DC (2019). Development and Validation of an HPLC Method for Simultaneous Assay of Potassium Guaiacolsulfonate and Sodium Benzoate in Pediatric Oral Powder. *J Anal Methods Chem*.

Mahdi WA, Bukhari SI, Imam SS, Alshehri S, Zafar A, et al. (2021). Formulation and optimization of butenafine-loaded topical nano lipid carrier-based gel: Characterization, irritation study, and anti-fungal activity. *Pharmaceutics* **13**(7).

Ogidi CO, Ojo AE, Ajayi-Moses OB, Aladejana OM, Thonda OA, et al. (2021). Synergistic antifungal evaluation of over-the-counter antifungal creams with turmeric essential oil or Aloe vera gel against pathogenic fungi. *BMC Complement Med Ther* **21**(1): 1–12.

Patel NA, Patel NJ, Patel RP (2009). Formulation and evaluation of curcumin gel for topical application. *Pharmaceutical Development and Technology* **14**(1): 83–92.

Pozharani LB, Baloglu E, Suer K, Guler E, Burgaz EV, et al. (2023). Development and optimization of in-situ gels for vaginal delivery of metronidazole and curcumin via box-behnken design: In vitro characterization and anti-trichomonas activity. *J Drug Deliv Sci Technol* **86**(7): 104739.

Pozharani LB, Burgaz EV, Baloğlu E (2022). Development and validation of an RP-HPLC method for simultaneous determination of curcumin and metronidazole in combined dosage form. *Istanbul J Pharm **52***(3): 250–257.

Research Article EMUJPharmSci ISSN 2651-3587 https://dergipark.org.tr/emujpharmsci

EMU Journal of Pharmaceutical Sciences

EMUJPharmSci

Computational Evaluation of Phytochemicals from *Chamaecyparis obtusa* var. *formosana* as Potential HSP90 Inhibitors

Taner Erdogan[1]*

[1] Kocaeli University, Department of Chemistry and Chemical Processing Technologies, Kocaeli Vocational School, Kocaeli, Türkiye.

Abstract

The identification of novel inhibitors targeting Heat Shock Protein 90 (HSP90) remains a promising strategy in anticancer drug discovery. In this study, three natural compounds from *Chamaecyparis obtusa* var. *formosanarecently*, which have recently been introduced in the literature, were subjected to a comprehensive computational investigation, including Density Functional Theory (DFT) calculations, molecular docking studies, molecular dynamics (MD) simulations and binding free energy calculations. DFT calculations were employed to optimize molecular geometries and generate molecular electrostatic potential (MEP) maps. Molecular docking studies were then performed to evaluate the interaction profiles of the compounds with HSP90. Following molecular docking studies, molecular dynamics (MD) simulations were conducted to assess the stability of the ligand–protein complexes and to determine the binding free energies using the MM-PBSA (Molecular Mechanics Poisson-Boltzmann Surface Area) method. MD simulations corroborated the formation of stable ligand-receptor complexes, as all three compounds maintained structural stability throughout the simulation period. Remarkably, two of the investigated compounds exhibited a higher binding affinity than the reference molecule, BIIB021 suggesting enhanced inhibitory potential. These results highlight the potential of the studied natural compounds as promising HSP90 inhibitors and provide a solid foundation for future experimental validation and drug development efforts.

Keywords

Cancer, computer aided drug design, HSP90, MD simulations, molecular docking, MM-PBSA.

Article History

Submitted: 08 December 2025 Accepted: 18 December 2025 Published Online: December 2025

Article Info

***Corresponding author:** Taner Erdogan **email:** taner.erdogan@kocaeli.edu.tr

Research Article:

Volume: 8 Issue: 3 Pages: 153-168

DOI: 10.54994/emujpharmsci.1838604

INTRODUCTION

Cancer is principally defined as a complex group of diseases characterized by the uncontrolled growth and spread of abnormal cells. In contrast to the regulation of cell division in normal biological processes, cancer is characterized by a disruption of the regulatory mechanisms that control the cell cycle and apoptosis. This loss of regulation enables uncontrolled proliferation of cells, resulting in invasion of adjacent tissues and subsequent dissemination to distant organs. Representing one of the most formidable challenges in modern medicine, it is a leading cause of morbidity and mortality worldwide. Despite significant progress in understanding tumor biology, the complexity and heterogeneity of cancer remain major challenges for global health.

At present, the therapeutic landscape for cancer comprises a wide range of modalities. Conventional therapeutic modalities, including surgery, chemotherapy, and radiotherapy, continue to serve as the primary treatment modalities. In recent years, these have been augmented by more advanced strategies, including immunotherapy, hormonal therapy, and targeted molecular therapies. While these interventions have led to improvements in survival rates for numerous malignancies, they are frequently constrained by limitations such as non-specific toxicity, the emergence of multi-drug resistance, and severe adverse effects. Consequently, there is an urgent and continuous need to identify novel therapeutic targets and develop more effective, less toxic agents.

In the search for targeted therapies, HSP90 has emerged as a promising candidate. HSP90 is a molecular chaperone that is found in all cell types and is involved in the maturation, stability, and activation of a variety of client proteins. In the context of cancer, HSP90 is of particular interest because many of its client proteins are oncogenic signaling molecules required for tumor growth, survival, and metastasis. Due to its therapeutic potential, the inhibition of HSP90 has been extensively studied (Abbasi et al. 2025; Erdogan, 2019; Erdogan and Oguz Erdogan, 2024, 2025; Farghaly et al. 2026; Nghakliana et al. 2025; Odabasoglu et al. 2022; Parveen et al. 2025; Srivastava et al. 2025; Yang et al. 2025; Zang et al. 2025)

Natural products continue to be a cornerstone in modern drug discovery, offering distinct chemical diversity and privileged scaffolds that are often challenging to synthesize in the laboratory. Endemic plant species serve as unique biological reservoirs, often harboring distinct chemical scaffolds with untapped

pharmacological potential. Among these, *Chamaecyparis obtusa* var. *formosana* is one of the important biological sources. While recent studies on this plant have successfully identified novel three natural compounds (Chang et al. 2025), these structures remain scientifically unexplored. To date, neither experimental bioassays nor theoretical calculations have been reported for these newly introduced molecules in the literature. This complete lack of data presents a compelling opportunity for investigation on HSP90 inhibition potentials of these natural compounds.

Motivated by the need to investigate potential biological activities of these newly isolated structures, in the present study, a comprehensive *in silico* approach was used to evaluate the HSP90 inhibitory potential of natural compounds derived from *Chamaecyparis obtusa* var. *formosana*. Specifically, DFT calculations, molecular docking, MD simulations, and binding free energy calculations were used to analyze the interactions and stability of these phytocompounds within the HSP90 active site. The results demonstrated that two of the investigated compounds (C.02 and C.03) exhibited higher binding affinities compared to the reference molecule, BIIB021.

MATERIALS AND METHODS

DFT calculations

The molecular structures of the investigated natural compounds (Figure 1) were initially retrieved from the literature (Chang et al. 2025). The three-dimensional structures were generated and subsequently optimized through DFT calculations. DFT calculations were carried out using B3LYP (Becke, three-parameter, Lee-Yang-Parr hybrid functional) functional in combination with 6-311+G(d,p) basis set. The solvent effects were accounted for using the SMD solvation model with water selected as the solvent. Gaussian (Frisch et al. 2016) was used in the DFT calculations, and GaussView (Roy Dennington et al. 2016) and Discovery Studio Visualizer (BIOVIA, 2023) were employed for the visualization of the results.

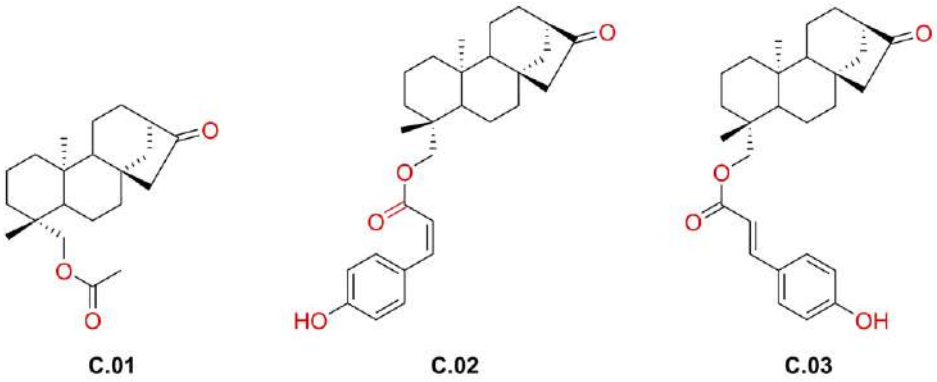

Figure 1: Molecular structures of the investigated compounds (Chang et al. 2025).

Molecular docking studies

The three-dimensional structure of the target protein, HSP90, was obtained from RCSB Protein Data Bank (PDB ID: 3QDD) (*www.rcsb.org*). The preparation of the protein and ligand structures was carried out using AutoDock Tools (Morris et al. 2009). Prior to docking calculations, a grid box was generated to encompass the active site of the HSP90 with the following parameters: center_x = -6.269, center_y = 33.666, center_z = 24.309, size_x = 22.500, size_y = 14.250, size_z = 17.250, spacing = 0.375, and exhaustiveness = 50. The docking protocol was validated by re-docking the original ligand, BIIB021. The molecular docking calculations were performed using AutoDock Vina (Trott and Olson, 2010). The most favorable binding poses were identified based on binding affinity scores, and the corresponding ligand-receptor complexes were obtained.

MD simulations and binding free energy calculations

To investigate the stability and dynamic behavior of the ligand-protein complexes, MD simulations were performed using GROMACS (Abraham et al. 2023; Van Der Spoel et al. 2005). The protein topology was generated using the AMBER force field (Duan et al. 2003), while the ligand parameters and topologies were obtained using the ACPYPE tool (Sousa Da Silva and Vranken, 2012). The system was solvated within a dodecahedron box, employing the TIP3P water model, and neutralized through the incorporation of Na^+ and Cl^- ions. Prior to the initiation of the MD run, energy minimization was applied to the system to remove steric clashes. The system was then subjected to 200 ps NVT and NPT ensemble equilibrations. Subsequently, a 100 ns MD simulation was carried out for each complex. The binding free energy was calculated for each complex using the MM-PBSA method and g_mmpbsa tool (Kumari et al. 2014). These calculations were performed based on the final 20ns of the MD simulation.

RESULTS AND DISCUSSIONS

DFT calculations

The optimized molecular structures of the compounds were obtained with the use of B3LYP/6-311+G(d,p) level of theory. No imaginary frequencies were observed in the vibrational analysis, confirming that the optimized geometries correspond to true local minima on the potential energy surface. Geometry optimized structures of the compounds are presented in Figure 2.

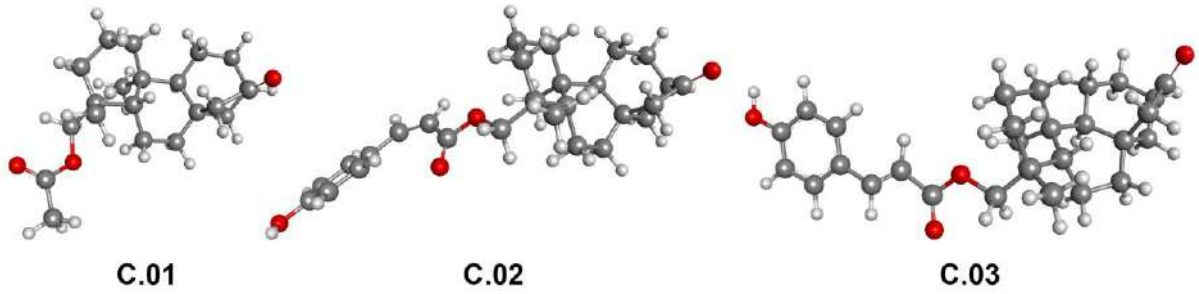

Figure 2: Geometry optimized structures of the investigated compounds.

Molecular Electrostatic Potential (MEP) maps were generated to visualize the charge distribution and the electrostatic nature of the studied compounds. In the context of structure-based drug design, MEP surfaces are essential for understanding the electrostatic complementarity between the ligand and the target protein. They allow for the identification of key structural features responsible for forming non-covalent interactions, such as hydrogen bonds within the active site. MEP maps of the investigated compounds are presented in Figure 3.

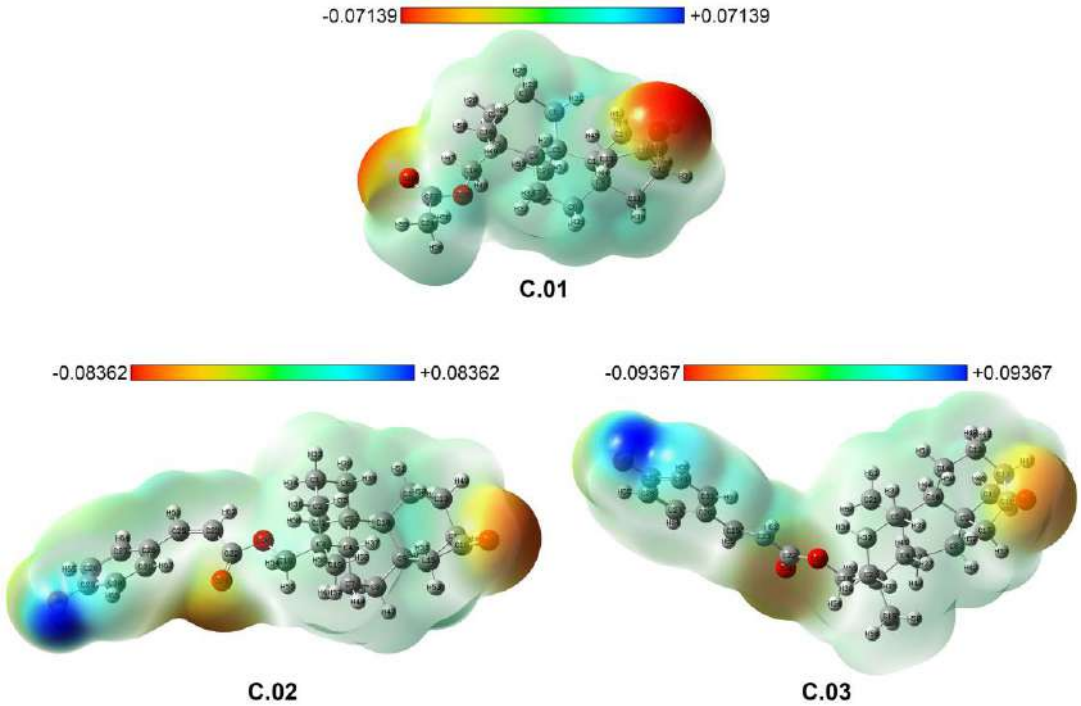

Figure 3: MEP maps of the investigated compounds.

The results demonstrated that negative electrostatic potential was predominantly concentrated over the oxygen atoms of the carbonyl groups. In contrast, particularly for compounds C.02 and C.03, the regions of positive electrostatic potential were localized on the hydrogen atoms of the hydroxyl groups, as theoretically expected.

Molecular docking studies

Molecular docking studies were carried out to investigate the binding conformations and the specific non-covalent interactions of the studied compounds within the active site of HSP90. Visual analysis of the docked poses confirmed that all three compounds (C.01, C.02 and C.03) fit well within the binding pocket, displaying a diverse network of interactions (Figure 4). According to molecular docking studies, the stability of C.01 within the active site was observed to be driven primarily by hydrophobic forces and weak hydrogen bonding. The interaction diagrams (Figure 5) highlighted the presence of carbon hydrogen bonds, alongside significant alkyl and π-alkyl interactions. These hydrophobic contacts suggest that the aliphatic and aromatic moieties of C.01 are well-embedded in the hydrophobic regions of the HSP90 pocket. The AutoDock Vina docking score for C.01 was determined to be -6.970 kcal/mol. C.02 exhibited a more complex interaction profile. Similar to C.01, it displayed carbon hydrogen bonds, alkyl, and π-alkyl interactions. However, a distinguishing feature of C.02 was the formation of π-π stacked interactions. This suggests that the aromatic rings of C.02 are positioned in parallel alignment with the aromatic amino acid residues of HSP90, providing additional stabilization to the complex. The AutoDock Vina docking score for C.02 was determined to be -10.050 kcal/mol. In the case of C.03, the binding mode was dominated by strong aromatic interactions. The analysis revealed a combination of π-π stacked and π-π T-shaped interactions, in addition to the standard alkyl and π-alkyl contacts. The presence of T-shaped interactions indicates a specific orthogonal orientation of the ligand's aromatic rings relative to the receptor's residues. The AutoDock Vina docking score for C.03 was determined to be -9.267 kcal/mol.

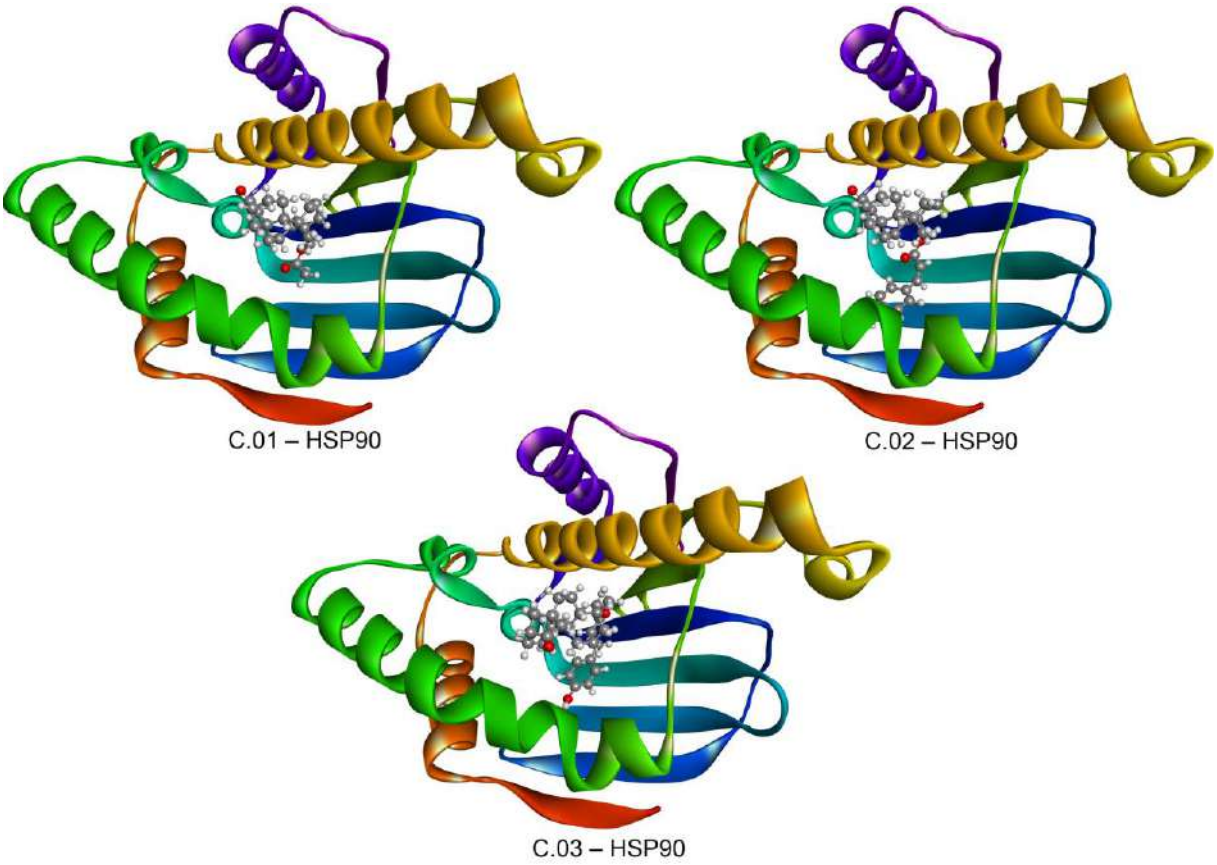

Figure 4: Binding poses obtained from molecular docking calculations.

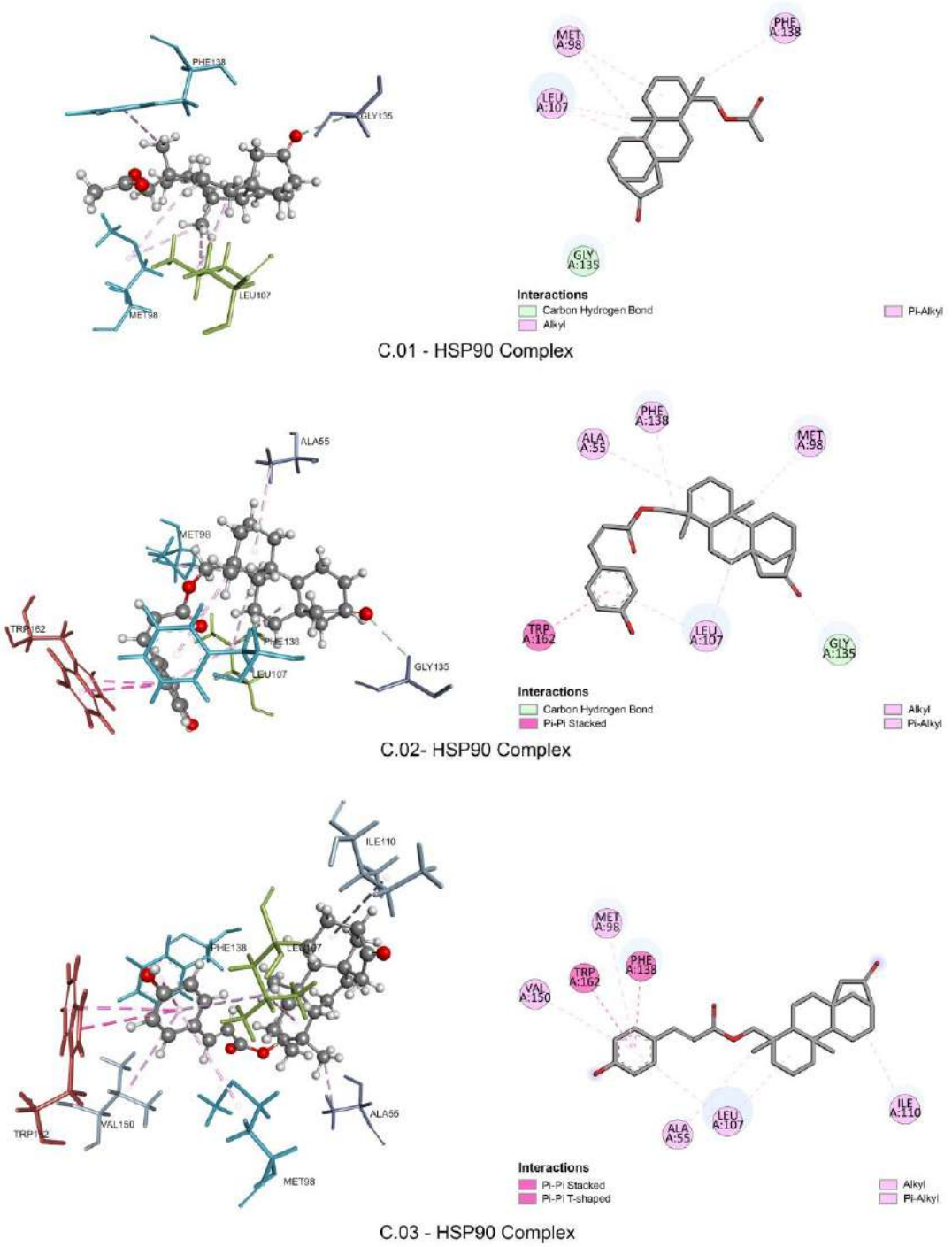

Figure 5: Ligand-receptor interactions between investigated compounds and HSP90.

MD simulations and binding free energy calculations

To evaluate the dynamic stability of the docked complexes and to ascertain the positional reliability of the ligands within the binding pocket, 100 ns MD simulations were performed. The results regarding the Root Mean Square Deviation (RMSD) are presented in Figure 6. Figure 6 compares the global stability (RMSD of complex after least squares fit to complex) and the ligand binding stability (RMSD of ligand after least squares fit to receptor).

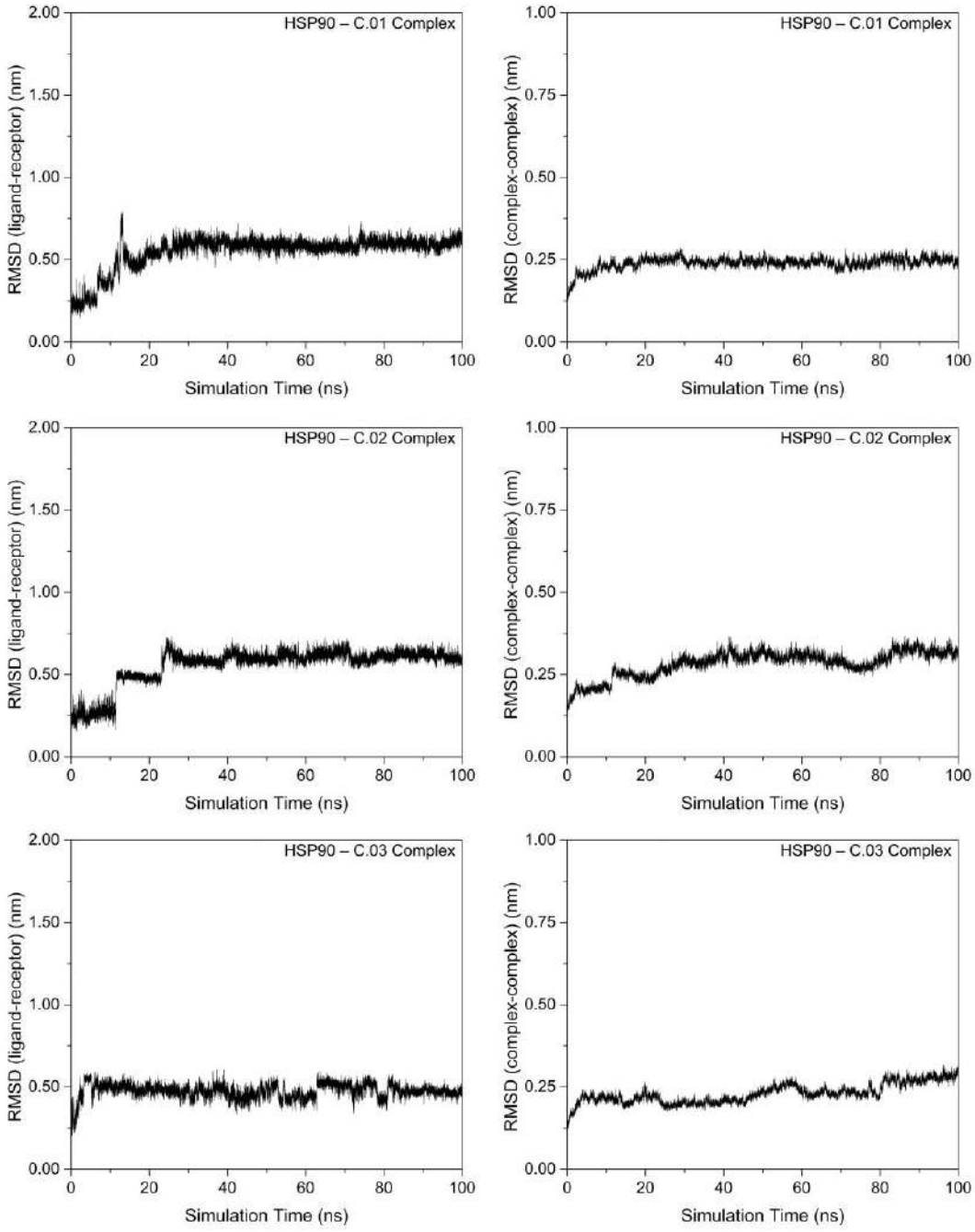

Figure 6: RMSD analysis of the ligand-receptor complexes.

The structural stability was primarily assessed using two distinct RMSD metrics. First, the RMSD of the complex (after least squares fit to the complex) was calculated to monitor the global equilibrium of the system. As observed in the plots, the complex RMSD values reached a plateau after the initial equilibration phase (after 20^{th} ns of the simulation for C.01, after 25^{th} ns for C.02, after 5^{th} ns for C.03), indicating that the overall protein-ligand systems remained stable without undergoing significant structural changes. Crucially, the RMSD of the ligand (after least squares fit to the receptor) was analyzed to specifically investigate the behavior of the ligand within

the binding pocket. This metric serves as a vital indicator of whether the ligand maintains its docking pose or undergoes significant translational and rotational shifts relative to the active site. The results demonstrated that the studied ligands exhibited low and stable RMSD values in this calculation, confirming that they remained tightly anchored within the binding pocket throughout the simulation period.

To further corroborate the formation of stable complexes, the Radius of Gyration (RG) of the receptor was examined (Figure 7). RG is a measure of compactness of the protein structure. The analysis revealed that the RG values remained relatively constant with minimal fluctuations, suggesting that the binding of the ligands did not induce any structural expansion or destabilization of the HSP90 protein structure. Finally, the intermolecular interactions were monitored by analyzing the number of hydrogen bonds formed between the ligand and the receptor during each MD simulation (Figure 7).

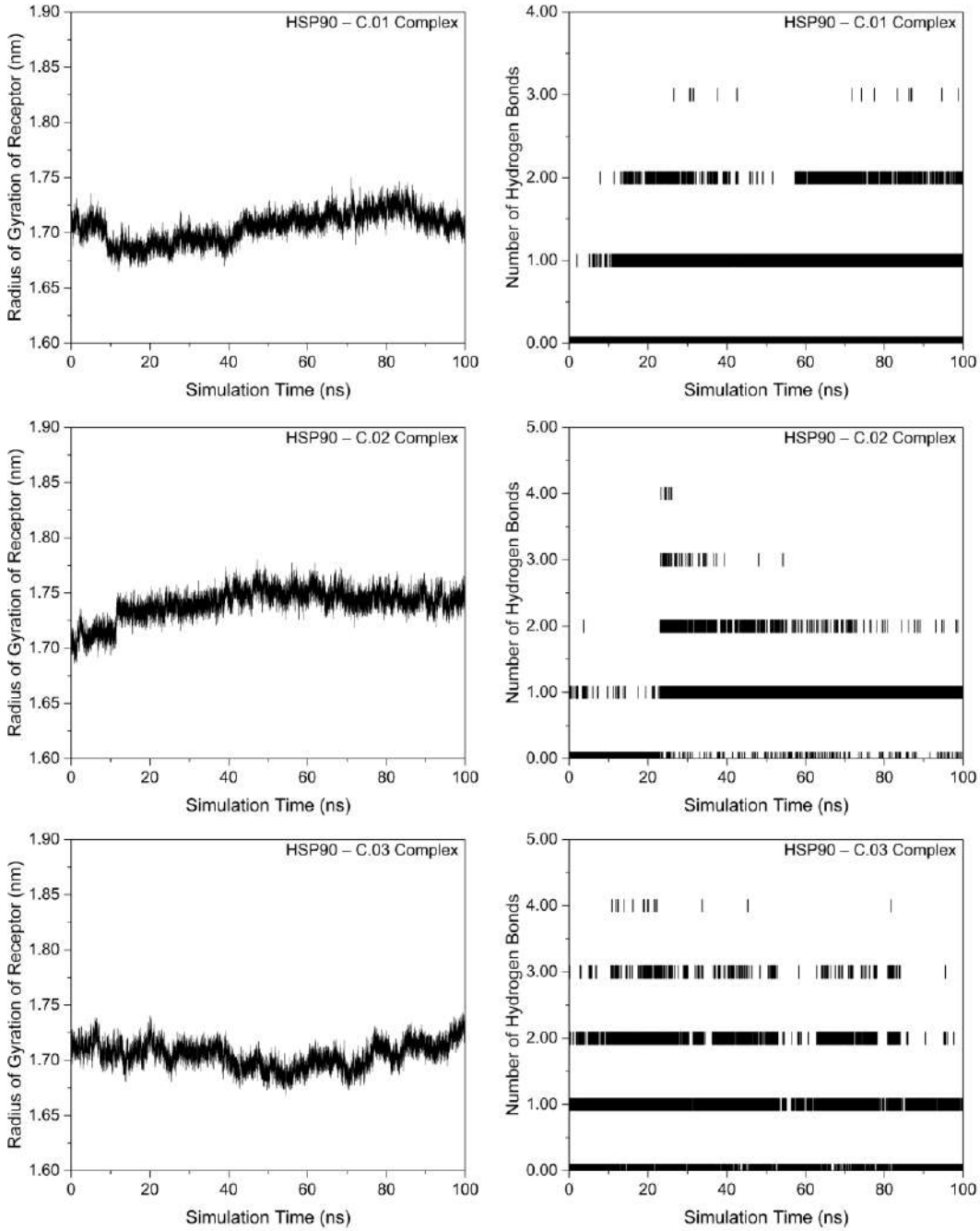

Figure 7: Radius of Gyration (RG) of receptor and number of hydrogen bonds formed between the ligand and the receptor for each ligand-receptor complex during the simulation.

While molecular docking provides a preliminary estimation of binding pose and affinity, MM-PBSA calculations following the MD simulations offer a more rigorous and quantitative assessment of the thermodynamic stability of the ligand-receptor complexes. To validate the docking findings and strictly compare the potency of the identified compounds against the reference inhibitor, BIIB021, the binding free energies were calculated using the stable trajectories from the last 20 ns of the MD simulations. The comparative results are presented in Figure 8. Binding free energy calculations with the use of MM-PBSA method revealed that two of the three

investigated phytochemicals possess superior binding affinities compared to the reference molecule BIIB021. As presented in Figure 8, the reference molecule exhibited a binding free energy of -28.6 kcal/mol, which was obtained from our previous study (Erdogan and Oguz Erdogan, 2025). In contrast, C.03 and especially C.02 displayed significantly lower (more negative) binding energies of -32.7 kcal/mol and -41.7 kcal/mol, respectively. This substantial difference in binding energy indicates that these natural compounds form much more stable complexes with the HSP90 than the known inhibitor, BIIB021. The third compound, C.01, also showed a favorable binding profile with a $\Delta G_{binding}$ of -23.1 kcal/mol, which was moderately lower than that of the reference molecule. The fact that these compounds achieved binding energies superior to the reference molecule, BIIB021, strongly suggests their potential as highly effective lead candidates for HSP90 inhibition.

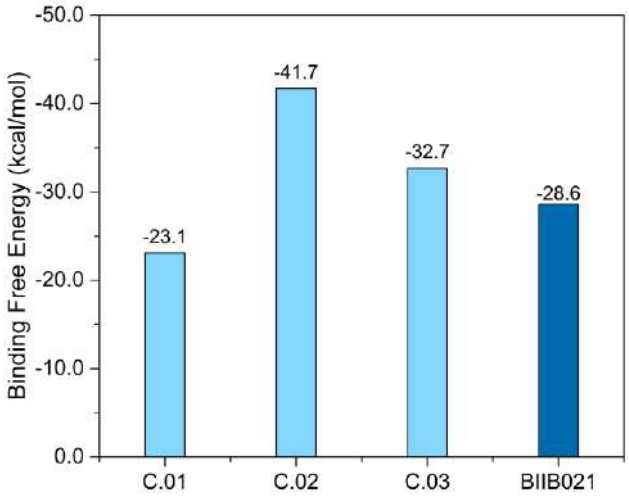

Figure 8: Comparison of MM-PBSA binding energies for the studied phytochemicals and reference molecule, BIIB021.

To elucidate the specific binding mechanisms and identify the key amino acid residues responsible for the high affinity of the studied compounds, a per-residue binding free energy decomposition analysis was conducted. The top contributing residues for each system are listed in Table 1. The three molecules exhibited distinctly different binding strategies, which can be categorized based on their dominant interaction profiles. C.02 demonstrated a pronounced reliance on aromatic residues for binding stabilization. The interaction landscape was dominated by an extensive network of aromatic amino acids PHE138, TRP162, TYR139, PHE22 and PHE170 and supporting hydrophobic residues, LEU107, LEU48, ILE26, VAL150. This binding profile suggests that C.02 achieves its high affinity through

extensive π-π stacking interactions and hydrophobic packing within the aromatic sub-pocket of HSP90. The presence of five aromatic residues among the top ten contributors indicates that aromatic complementarity is the primary driving force for this compound's binding mode.

In contrast to the aromatic-dominant profile of C.02, C.01 displayed a distinct binding mode driven largely by hydrophobic residues. The highest energy contributions for C.01 came from ILE110, ALA55, and MET98. Furthermore, the presence of polar and charged residues such as ASN106, THR184, GLU62, and ASP57 in the top ten list indicates that C.01 relies on a combination of shape complementarity with aliphatic side chains and specific electrostatic interactions, representing a mechanistically different approach compared to C.02.

C.03 exhibited a hybrid interaction profile that uniquely combines elements from both binding strategies observed in C.01 and C.02. This compound engages both the aromatic sub-pocket and the aliphatic hydrophobic core of the HSP90 binding site. C.03 achieves a balanced engagement strategy that allows it to maximize contacts across different regions of the active site. The presence of SER52 suggests that polar interactions further stabilize this dual-mode binding.

Significantly, per-residue decomposition analysis indicated that residues including ILE110, ALA55, MET98, LEU107, THR184, PHE138, and LEU48 made major contributions to the binding energy. These residues have previously been reported as key interaction sites for HSP90 inhibition (Yan et al. 2020; Yi et al. 2010).

Table 1. The top ten amino acid residues contributing to the binding free energies for each ligand-receptor complex based on MM-PBSA decomposition analysis.

C.01-HSP90 Complex		**C.02-HSP90 Complex**		**C.03-HSP90 Complex**	
Residue	**Contribution (kcal/mol)**	**Residue**	**Contribution (kcal/mol)**	**Residue**	**Contribution (kcal/mol)**
ILE110	-1.9943	LEU107	-2.5905	MET98	-2.212
ALA55	-1.5214	PHE138	-2.2416	PHE138	-2.0206
MET98	-1.4815	TRP162	-1.7883	ILE110	-1.8166
LEU107	-1.0822	TYR139	-1.5654	LEU107	-1.5336
SER52	-0.8741	ILE26	-0.9595	ALA55	-1.0935
ASN106	-0.6681	VAL150	-0.9367	TRP162	-0.8807
ILE96	-0.6398	PHE22	-0.9248	ILE96	-0.7235
THR184	-0.5925	LEU48	-0.875	VAL150	-0.5331
GLU62	-0.3515	GLY108	-0.8262	SER52	-0.5175
ASP57	-0.3408	PHE170	-0.7919	TYR139	-0.4083

CONCLUSION

In this study, a comprehensive *in silico* framework combining DFT, molecular docking, MD simulations, and MM-PBSA binding free energy calculations were employed to identify potent HSP90 inhibitors from the bioactive constituents of *Chamaecyparis obtusa* var. *formosana*. The quantum chemical calculations at DFT level were initially utilized to obtain fully optimized molecular geometries and to elucidate the electronic properties of the compounds. Molecular docking studies demonstrated that the investigated phytochemicals occupied the ATP-binding pocket of HSP90 with favorable binding poses. The stability of these complexes was further validated by 100 ns MD simulations. The analyses of RMSD, RG, and hydrogen bond dynamics confirmed that the ligands remained tightly anchored within the binding pocket without inducing significant conformational changes in the protein structure. Most significantly, the quantitative binding free energy calculations using the MM-PBSA method highlighted the superior potential of two specific compounds (**C.02** and **C.03**). These candidates exhibited stronger binding affinities (more negative $\Delta G_{binding}$ values) compared to the reference inhibitor, BIIB021. This thermodynamic advantage suggests that these natural derivatives could offer higher efficacy and stability as HSP90 inhibitors. Collectively, the results of this study provide strong theoretical evidence supporting the HSP90 inhibition potential of natural compounds from *Chamaecyparis obtusa* var. *formosana*. The identified compounds stand out as promising lead candidates for the development of novel HSP90 inhibitors, warranting further *in vitro* and *in vivo* experimental validation.

ACKNOWLEDGEMENTS

The computational studies reported in this paper were partially performed at TUBITAK ULAKBIM, High Performance and Grid Computing Center (TRUBA resources), and Kocaeli University.

REFERENCES

Abbasi M, Talaei S, Farshidfar G (2025). Prediction of new C-terminal Hsp90 inhibitors based on deguelin scaffold: homology modeling, virtual screening, QM/MM docking, MM/GBSA, and molecular dynamics simulations. *Research in Pharmaceutical Sciences* **20**(6): 824–835.

Abraham M, Alekseenko A, Bergh C, Blau C, Briand E, et al. (2023), *GROMACS* **3** *Source code*.

BIOVIA DS (2023). Discovery Studio Modeling Environment, Release v24.1.0.23298, San Diego: Dassault Systèmes, 2023.

Chang CI, Chan YF, Kuo CC, Kuo YH (2025). Three new ent-17-norkaurane diterpenoids from the leaves of Chamaecyparis obtusa var. formosana and their cytotoxic activity against HONE-1 human carcinoma cell lines. *Phytochem Lett* **70*:*** 104050.

Duan Y, Wu C, Chowdhury S, Lee MC, Xiong G, et al. (2003). A point-charge force field for molecular mechanics simulations of proteins based on condensed-phase quantum mechanical calculations. *Journal of Computational Chemistry* **24**(16): 1999–2012.

Erdogan T (2019). Synthesis, characterization, DFT and molecular docking studies for novel 1,5-diphenylpenta-1,4-dien-3-one O-benzyl oximes. *Journal of the Iranian Chemical Society 2019* **16**(10): 2243–2255.

Erdogan T, Oguz Erdogan F. (2024). Probing some recent natural compounds from Phellinus baumii, Colletotrichum sp. and Ligustrum lucidum as heat shock protein 90 inhibitors. *Journal of Biomolecular Structure and Dynamics* **42**(10): 5390–5401.

Erdogan T, Oguz Erdogan F (2025). Assessment of heat shock protein 90 and epidermal growth factor receptor inhibitory potential of natural compounds from Calophyllum membranaceum and Leonurus sibiricus via molecular dynamics simulations and binding free energy calculations. *Molecular Physics* e2475166,

Farghaly AM, AboulWafa OM, Baghdadi HH, Abd El Razik HA, Farag EMM, et al. (2026). New thieno[2,3-d]pyrimidinone-based derivatives: Design, synthesis, biological potential, and in silico studies against breast cancer. *Journal of Molecular Structure*, *1352*, 144530.

Frisch MJ, Trucks GW, Schlegel HB, Scuseria GE, Robb MA, et al. (2016). *Gaussian 16 Revision C.01*.

Kumari R, Kumar R, Lynn A (2014). G-mmpbsa -A GROMACS tool for high-throughput MM-PBSA calculations. *Journal of Chemical Information and Modeling* **54**(7): 1951–1962.

Morris GM, Huey R, Lindstrom W, Sanner MF, Belew RK, et al. (2009). AutoDock4 and AutoDockTools4: Automated docking with selective receptor flexibility. *J Comput Chem* **30**(16): 2785–2791.

Nghakliana F, Tochhawng L, Sailo H, Lalawmpuii R, Lalsangpuii F, et al. (2025). In Vitro Evaluation of Anticancer and Apoptotic Activity of Elaeagnus caudata Schltdl. With Computational Identification of a Novel HSP90 Inhibitor. *Chemistry and Biodiversity*.

Odabasoglu HY, Erdogan T, Karci F (2022). Synthesis & characterization of heterocyclic disazo - azomethine dyes and investigating their molecular docking & dynamics properties on acetylcholine esterase (AChE), heat shock protein (HSP90α), nicotinamide N-methyl transferase (NNMT) and SARS-CoV-2. *Journal of Molecular Structure* **1252**: 131974.

Parveen S, Kumar RS, Rathi A, Nayeem A, Qais FA, et al. (2025). In Silico Investigation of Eleusine coracana Phytocompounds as Prostate Cancer Therapeutics Targeting Heat Shock Protein 90 Alpha Family Protein. *Journal of Computational Biophysics and Chemistry* **24**(7): 933–948.

RCSB PDB. (2021) https://www.rcsb.org/ Accessed: 14.10.2025.

Dennington R, Keith AT, Millam JM (2016). *GaussView 6*. Semichem Inc.

Sousa Da Silva AW, Vranken WF (2012). ACPYPE - AnteChamber PYthon Parser interfacE. *BMC Research Notes* **5**(1): 367.

Srivastava S, Upadhyay HC, Goswami P, Koch B, Maurya HK, et al. (2025). Design, In Silico Screening, Synthesis, and In Vitro Assessment of 1,4-Naphthoquinone-Tethered Hybrid Molecules to Explore Their Anticancer and Antimicrobial Potential. *ACS Omega* **10**(36): 41158–41173.

Trott O, Olson AJ (2010). AutoDock Vina: Improving the speed and accuracy of docking with a new scoring function, efficient optimization, and multithreading. *Journal of Computational Chemistry* **31**(2): 455–461.

Van Der Spoel D, Lindahl E, Hess B, Groenhof G, Mark AE, et al. (2005). GROMACS: Fast, flexible, and free. *Journal of Computational Chemistry* **26**(16): 1701–1718.

Yan F, Liu X, Zhang S, Zhang Q, Chen J (2020). Understanding conformational diversity of heat shock protein 90 (HSP90) and binding features of inhibitors to HSP90 via molecular dynamics simulations. *Chemical Biology and Drug Design* **95**(1), 87–103.

Yang S, Zhou X, Xin X, Lu Y, Zhang Z, et al. (2025). Elucidating Hsp90α/β selectivity mechanisms via computer-aided drug design. *Molecular Simulation*.

Yi CH, Chen JZ, Shi SH, Hu GD, Zhang QG (2010). A computational analysis of pyrazole-based inhibitors binding to Hsp90 using molecular dynamics simulation and the MM-GBSA method. *Molecular Simulation* **36**(6): 454–460.

Zang M, Gan H, Zhou X, Wang L, Dong H (2025). Dual-Site Targeting by Peptide Inhibitors of the N-Terminal Domain of Hsp90: Mechanism and Design. *Journal of Chemical Information and Modeling* **65**(10): 5113–5123.

Review EMUJPharmSci ISSN 2651-3587 https://dergipark.org.tr/emujpharmsci

EMU Journal of Pharmaceutical Sciences

EMUJPharmSci

Chemotherapy and Personalized Medicine: New Approaches in Modern Cancer Treatment

Imge Kunter [1]

[1]Eastern Mediterranean University, Faculty of Pharmacy, Famagusta, North Cyprus via Mersin 10, Türkiye.

Abstract

Chemotherapy has been an important part of cancer treatment for many years. However, its efficacy is often limited because conventional chemotherapy can cause serious side effects and lead to differences in treatment response between patients. At this point, personalized medicine offers a new approach to eliminating these problems in cancer treatment. Personalized medicine proposes organizing treatment according to the genetic and molecular characteristics of both the tumor and the patient with tailored treatment regimens. Through molecular profiling of the patient and the tumor, oncologists can have a preliminary idea about the most effective drug, allowing them to adjust the treatment specifically for the individual and minimize the harmful effects on healthy tissues. Advances in genomics and precision oncology, and also new platforms such as organoids and organ-on-chips, have made it possible to select drugs, based on tumor-specific biomarkers, genomic alterations, and pharmacogenomic variants. However, there are still some challenges in applying personalized chemotherapy. Major challenges include concerns about the reliability of biomarkers, integration of genomic data into clinical practice, cost-effectiveness, and ethical issues related to genetic privacy. This review summarizes the basic concepts of tumor biology and chemotherapy and discusses how personalized medicine and precision oncology are changing cancer treatment.

Keywords

Chemotherapy, personalized medicine, pharmacogenomics, precision oncology.

Article History

Submitted: 05 December 2025 Accepted: 19 December 2025 Published Online: December 2025

Article Info

***Corresponding author:** Imge Kunter **email:** imge.kunter@emu.edu.tr

Review:

Volume: 8 Issue: 3 Pages: 169-178

DOI: 10.54994/emujpharmsci.1836760

INTRODUCTION

Chemotherapy, as a cornerstone of cancer treatment, has traditionally been administered and widely used based on standard protocols and general guidelines. However, because it cannot precisely target specifically cancer cells, it has a high risk of damaging healthy tissues because of the toxic side effects and also results in large differences in treatment response between patients, which in turn affects patient's quality of life and overall well-being. For example, while the same dose of cisplatin may cause minimal toxicity in some patients, it can lead to severe neurotoxicity or nephrotoxicity in others. These differences are primarily attributed to genetic variations and differences in drug metabolism. (Zazuli et al. 2018; Trendowski et al. 2019) The concept of personalized medicine aims to reduce these problems by adjusting therapy according to the molecular and genetic characteristics of both the tumor and the patient. (Zhao et al. 2025; Qiao et al. 2025). By identifying patients who are less likely to benefit from conventional chemotherapy regimens, alternative treatment options can be explored, such as targeted therapies or immunotherapies.

Personalized medicine, by tailoring chemotherapy to an individual's genetic makeup, helps minimize damage to healthy cells and facilitates better treatment outcomes. Thanks to technological advances such as next-generation sequencing (NGS), organoid models, and liquid biopsies, targetable mutations and tumor heterogeneity can be more easily identified and used to shape treatment strategies. (Ghoreyshi et al. 2025) In this way, oncology is shifting from a “one-size-fits-all” approach to a more predictable and personalized discipline.

However, it should not be overlooked that, despite the great potential of personalized chemotherapy, there are various challenges and obstacles, such as ethical issues related to genetic data, the integration of genomic information into clinical practice, and the development of affordable diagnostic tests. This review will focus on how tumor biology forms the basis of personalized chemotherapy strategies and highlights the importance of molecular profiling and pharmacogenomics in this context while discussing the drawbacks of these concepts.

Fundamentals of tumor biology

Initiation, development and classification of tumors

Tumors are structures that arise when normal cells begin uncontrolled proliferation as a result of various biological or environmental factors, and they can be either benign or malignant. Benign tumors remain in the tissue and do not spread, whereas malignant tumors can invade surrounding tissues and can metastasize to distant organs.

Tumors are classified according to the type of tissue from which they derive. Epithelial tissue originating malignant tumors are classified as carcinomas, whereas those developing from connective tissues are known as sarcomas. Imaging techniques (CT, MRI, ultrasound) and histopathological examination of biopsy specimens contribute to the diagnosis. TNM staging is the system used to determine how far the tumor has spread in the body. In this system, tumor size (T), involvement of lymph nodes (N), and the presence of metastasis (M) are evaluated. This information plays a crucial role in designing the treatment plan. (Klug et al. 2025) Due to technological advances and the growing molecular cancer knowledge in the literature, molecular pathology has now added genomic subtypes to this classification, allowing treatment selection to be performed more effectively. Validated molecular tests have enabled tumors to be classified in much greater detail in addition to the classical histopathological classification. Through these analyses, key features of biopsy tissues—such as driver mutations (e.g., EGFR, KRAS, BRAF), DNA damage repair defects (BRCA mutations, HRD, MSI-H/MMR deficiency), gene fusions (ALK, NTRK, RET), copy-number alterations (HER2 amplification), and gene expression profiles—can be evaluated together, leading to more precise tumor typing. As a result, tumors can be classified not only according to their tissue of origin but also according to their genetic mutation patterns, activated signaling pathways, immunologic characteristics, and transcriptomic subtypes. This type of molecular classification strengthens our understanding of tumor biology and contributes significantly to the better selection of targeted therapies for personalized treatment approaches. (Wang et al. 2025; Grodzka et al. 2023; Yang et al. 2024)

Molecular hallmarks of cancer

Modern oncology considers cancer to be a multistep process that arises from the accumulation of genetic and epigenetic alterations**.** The hallmarks of cancer concept have shown us that malignant transformation is far more than a simple problem of uncontrolled proliferation. According to Hanahan and Weinberg, cancer cells

progressively acquire numerous functional capabilities during carcinogenesis, in various combinations, such as sustaining proliferative signaling, evading growth suppressors, resisting cell death, enabling replicative immortality, inducing angiogenesis, initiating invasion and metastasis, reprogramming cellular metabolism, and avoiding immune destruction. These biological acquisitions of cancer cells are now understood to be facilitated by processes such as genomic instability and tumor-promoting inflammation, and further supported by newer dimensions including phenotypic plasticity, epigenetic reprogramming, and polymorphic microbiomes. Understanding all these processes is critical for identifying molecular targets for therapy. (Hanahan, 2022)

As new data continues to accumulate in the literature, our increasingly detailed molecular-level understanding of cancer has enabled the development of various targeted therapies. Many of these treatments are biological agents, with monoclonal antibodies in particular occupying a prominent role. Examples include trastuzumab, which targets HER2-mediated signaling in breast cancer; rituximab, which targets CD20 in B-cell lymphomas; bevacizumab, which neutralizes VEGF-A to suppress tumor angiogenesis; and cetuximab, which blocks EGFR signaling in colorectal and head-and-neck cancers. (Jin et al. 2025; Castillo et al. 2025; Mohan et al. 2021; Kaufman et al. 2021)

Relevance to targeted therapy

The fundamental molecular mechanism alterations present in an individual's cancer tissue are among the most critical factors explaining why chemotherapy response varies from one patient to another. DNA repair defects, proliferation patterns, metabolic reprogramming, and immune-evasion mechanisms are key molecular signatures that determine which therapies are effective.

Understanding the molecular features of cancer cells and how tumors behave helps oncologists target tumor vulnerabilities more effectively. For example, tumors with BRCA mutations respond well to platinum drugs and PARP inhibitors because their DNA repair system does not work properly. (Jin et al., 2025) In the same way, microsatellite instability (MSI) shows that the mismatch repair system is defective, which causes many mutations and the formation of many neoantigens. These neoantigens make the tumor easier for the immune system to recognize, so MSI-high tumors respond well

to immune checkpoint inhibitors (Fan et al. 2025).

Conventional chemotherapy: mechanisms and limitations

Conventional small-molecule chemotherapeutics are chemically synthesized cytotoxic agents that, unlike biological drugs, are not designed to target a specific molecular structure. These agents can be classified into groups such as antimetabolites (by disruping nucleotide synthesis), alkylating agents (by creating DNA crosslinks), platinum compounds (by forming DNA adducts and crosslinks that disrupt replication), topoisomerase inhibitors (by preventing DNA unwinding), and mitotic inhibitors (by interfering with microtubule dynamics). By disrupting DNA replication, inhibiting cell division, or targeting essential metabolic pathways, they eliminate tumor cells or inhibit their proliferation. Unfortunately, because these processes also occur in normal cells, chemotherapeutics are not selective and can affect rapidly dividing healthy tissues as well as cancer cells. Genetic variability and tumor heterogeneity lead to significant differences in treatment response among patients. Therefore, due to interpersonal genetic differences and tumor heterogeneity, determining which chemotherapeutic agent will be effective for a specific patient becomes challenging. (Tilsed et al. 2022)

While effective in many cancers, these agents lack specificity, often damaging normal proliferating tissues such as bone marrow and intestinal mucosa. This leads to common adverse effects like neutropenia, mucositis, and alopecia. Furthermore, pharmacogenetic variability in drug metabolism and tumor genetic diversity can result in unpredictable responses and resistance. (Emran et al. 2022; Anand et al. 2022)

The presence of cancer stem cells (CSCs), also a challenge and complicates treatment. CSCs are small but chemotherapy-resistant cell population with the ability to self-renew and repopulate the tumor after therapy. Since this cell subpopulation does not divide continuously, possesses enhanced DNA repair capacity, has well-developed drug efflux systems (such as ABC transporters), and exhibits resistance to apoptosis, it can resist conventional chemotherapy and is difficult to eradicate. As a result, because the rapidly dividing cancer cells are eliminated the tumor mass appears to respond quickly to the treatment, but CSCs can gain dominance and trigger tumor recurrence and metastatic spread. This CSC-mediated therapeutic resistance highlights the need for treatment strategies that target stem-like cell subgroups

in addition to the proliferating tumor mass. (Batlle and Clevers, 2017)

Precision oncology and molecular profiling

Molecular profiling reveals targetable mutations, gene expression patterns, and epigenetic alterations that can guide therapy selection (Malone et al. 2020). In breast cancer example, HER2 amplification justifies the use of trastuzumab, whereas in colorectal cancer, KRAS mutations exclude the use of EGFR inhibitors. NGS and circulating tumor DNA (ctDNA) analyses gather information on tumor progression and resistance mechanisms, which help to improve treatment strategies. (Bartolomucci et al. 2025) These tools are increasingly contributing to cancer therapy by evaluating therapeutic efficacy in both clinical trials and routine practice.

For example, in the diagnosis and treatment of ovarian cancer, molecular profiling is an important illustration of how personalized chemotherapy can be guided. In ovarian cancer, patients with BRCA1/2 mutations and HRD (Homologous Recombination Deficiency) status benefit from platinum-based therapies and PARP inhibitors. (Moore et al. 2018) PD-L1 expression and tumor-infiltrating lymphocytes can guide immunotherapy selection, helping ensure that the patient receives the most effective treatment. (Martin de la Fuente et al. 2020)

However, despite the ability of molecular profiling to identify potential therapeutic targets, it does not always accurately predict how a tumor from a specific patient will respond to a specific chemotherapeutic agent. In such cases, the use of additional platforms, such as patient-derived organoids, contributes to more personalized chemotherapy. (Pernik et al. 2021)

Organoid models in personalized chemotherapy

Tumor-derived organoids are miniature models of the patient's own tumor and provide a new perspective for personalized chemotherapy. In these organoids, the patient's genetic background is preserved while the phenotypic characteristics, three-dimensional architecture, and cellular heterogeneity of the tumor are maintained in a highly realistic manner. By doing so, organoids not only reflect the behavior of individual cells alone but also successfully mimic the interactions among groups of tumor cells, intratumoral heterogeneity, spatial organization, cell–cell communication, and microenvironmental properties that influence drug response. For these reasons, organoids are far more suitable than conventional 2D cell lines for predicting

actual clinical response. Moreover, although it is not feasible to test multiple chemotherapeutic agents or complex drug combinations directly on a patient, organoids allow such regimens to be evaluated experimentally in the laboratory. When organoids are integrated with organ-on-chip technologies, they can also model specific aspects of the patient's systemic physiology. This technological combination enables dose optimization and the assessment of multidrug regimens in a physiologically meaningful and controlled environment. Considering patient-specific variability and tumor heterogeneity in cancer, therapeutic strategies will inevitably evolve towards these functional modeling systems to better guide individualized treatments. These technologies represent a promising step toward integrating personalized oncology into routine clinical practice. (Chitrangi et al. 2023; Kim et al. 2020; Ren et al. 2023; Yi et al. 2023)

Single-Cell sequencing and tumor heterogeneity

Single-cell sequencing is a new tool that makes it possible to identify cancer stem cell (CSC) populations by resolving a heterogeneous population at the single-cell level. This technology reveals the transcriptional profile of each cell, identifying gene signatures specific to CSCs, revealing important signaling pathways (Wnt, Notch, Hedgehog), and resistance mechanisms. Clinically, single-cell analyses identify therapy-resistant subclones and CSC-specific therapeutic targets, making it possible to choose personalized chemotherapy for the patient. (Li et al. 2024; Kim et al. 2018)

Pharmacogenomics in personalized chemotherapy

Pharmacogenomics is an approach that examines how individual genetic variations influence drug metabolism, drug-related toxicity, and therapeutic efficacy using different techniques. Several clinically meaningful examples demonstrate the importance of this approach. For instance, dihydropyrimidine dehydrogenase (DPYD) variants can increase the risk of fluoropyrimidine-related toxicity; thiopurine S-methyltransferase (TPMT) deficiency predisposes patients to severe thiopurine toxicity; uridine diphosphate-glucuronosyltransferase 1A1 (UGT1A1) polymorphisms affect the elimination of irinotecan; and excision repair cross-complementation group 1 (ERCC1) overexpression contributes to the development of resistance to platinum-based therapies (Amstutz et al. 2018; Relling and

Evans, 2015; de With et al. 2023). Despite the potential benefits of pharmacogenomic testing for guiding treatment, its integration into routine oncology practice remains challenging due to cost, limited access to technology, and insufficient clinical guidelines. Nevertheless, these tests are increasingly contributing to diagnostic and therapeutic decision-making in high-income countries.

Challenges and future directions

Personalized chemotherapy has the potential to avoid ineffective treatments, increase treatment response, and reduce toxicity; however, there are still important barriers. The lack of validated predictive biomarkers, the high cost of molecular diagnostic tests, infrastructure differences between healthcare systems, the absence of clear health regulations in different countries, and ethical concerns related to genetic data privacy and consent make the implementation of personalized chemotherapy difficult.

Personalized chemotherapy will be an approach that can greatly increase chemotherapy success rates in oncology. Adapting treatment strategies to the molecular signature of the tumor and the patient can provide higher effectiveness and fewer side effects. However, for this approach to be applied on a wider scale, challenges related to access, cost, and ethical management need to be overcome. For personalized chemotherapy to advance, multi-omics approaches integrating genomic, transcriptomic, proteomic, and metabolomic data, AI-supported clinical decision systems, global biomarker validation studies, and the development of clear health regulations are needed. In addition, updating the training of all stakeholders is essential. With technological progress and updated education and regulations, the integration of personalized chemotherapy as a standard approach in routine care seems highly achievable in the near future.

ACKNOWLEDGMENTS

The authors declare no conflict of interest.

REFERENCES

Amstutz U, Henricks LM, Offer SM, Barbarino J, Schellens JHM, et al. (2018). Clinical Pharmacogenetics Implementation Consortium (CPIC) guideline for dihydropyrimidine dehydrogenase genotype and fluoropyrimidine dosing: 2017 update. *Clin Pharmacol Ther* **103**(2): 210–216.

Anand U, Dey A, Chandel AKS, Sanyal R, Mishra A, et al. (2022). Cancer chemotherapy and beyond: Current status, drug candidates, associated risks and progress in targeted therapeutics. *Genes Dis* **10**(4): 1367–1401.

Bartolomucci A, Nobrega M, Ferrier T, et al. (2025). Circulating tumor DNA to monitor treatment response in solid tumors and advance precision oncology. *NPJ Precis Oncol* **9**: 84.

Batlle E, Clevers H (2017). Cancer stem cells revisited. *Nat Med* **23**(10): 1124–1134.

Castillo DR, Guo M, Shah P, et al. (2025). CLDN18.2 and PD-L1 profiling in gastric cancer. *Transl Oncol* **28**: 101065.

Chitrangi S, Vaity P, Jamdar A, Bhatt S (2023). Patient-derived organoids for precision oncology: A platform to facilitate clinical decision making. *BMC Cancer* **23**: 689.

de With M, van Doorn L, Kloet E, van Veggel A, Matic M, et al. (2023). Irinotecan-induced toxicity: A pharmacogenetic study beyond UGT1A1. *Clin Pharmacokinet* **62**: 1589–1597.

Emran TB, Shahriar A, Mahmud AR, Rahman T, Abir MH, et al. (2022). Multidrug resistance in cancer: Understanding molecular mechanisms, immunoprevention and therapeutic approaches. *Front Oncol* **12:** 891652.

Fan S, Qingyu M, Zhao Z, Niu W (2025). Long-term response in rare MSI-H CRC with BRAF mutation. *Front Immunol* **16**: 1698410.

Ghoreyshi N, Heidari R, Farhadi A, Chamanara M, Farahani N, et al. (2025). Next-generation sequencing in cancer diagnosis and treatment: Clinical applications and future directions. *Discov Oncol* **16**(1): 578.

Grodzka A, Knopik-Skrocka A, Kowalska K, Kurzawa P, Krzyżaniak M, et al. (2023). Molecular alterations of driver genes in non-small cell lung cancer: From diagnostics to targeted therapy. *EXCLI J* **22**: 415–432.

Hanahan D (2022). Hallmarks of cancer: New dimensions. *Cancer Discov* **12**(1): 31–46.

Jin H, Yang Y, Yan C, Liu M, Heet X, et al. (2025). Tumor immunophenotyping in HER2+ breast cancer. *Mol Cancer* **24**: 483.

Kaufman NEM, Dhingra S, Jois SD, Vicente MGH (2021). Molecular targeting of epidermal growth factor receptor (EGFR) and vascular endothelial growth factor receptor (VEGFR). *Molecules* **26**(4): 1076.

Kim C, Gao R, Sei E, Brandt R, Hartman J, et al. (2018). Chemoresistance evolution in triple-negative breast cancer delineated by single-cell sequencing. *Cell* **173**(4): 879–893.e13.

Kim J, Koo BK, Knoblich JA (2020). Human organoids: Model systems for human biology and medicine. *Nat Rev Mol Cell Biol* **21**: 571–584.

Klug M, Kirshenboim Z, Truong MT, Sorin V, Keren Gilat E, et al. (2025). The ninth edition TNM staging system for thymic epithelial tumors: A comprehensive review. *Radiol Cardiothorac Imaging* **7**(5).

Li R, Liu X, Huang X, Zhang D, Chen Z, et al. (2024). Single-cell transcriptomic analysis deciphers heterogenous cancer stem-like cells in colorectal cancer and their organ-specific metastasis. *Gut* **73**(3): 470–484.

Malone ER, Oliva M, Sabatini PJB, Stockley TL, Siu LL (2020). Molecular profiling for precision cancer therapies. *Genome Med* **12**(1): 8.

Martin de la Fuente L, Westbom-Fremer S, Arildsen NS, Hartman L, Malander S, et al. (2020). PD-1/PD-L1 expression and tumor-infiltrating lymphocytes are prognostically favorable in advanced high-grade serous ovarian carcinoma. *Virchows Arch* **477**(1): 83–91.

Mohan N, Luo X, Shen Y, Olson Z, Agrawal A, et al. (2021). A novel bispecific antibody targeting EGFR and VEGFR2 is effective against triple negative breast cancer via multiple mechanisms of action. *Cancers* **13**(5): 1027.

Moore K, Colombo N, Scambia G, Kim B-G, Oaknin A, et al. (2018). Maintenance olaparib in newly diagnosed advanced ovarian cancer. *N Engl J Med* **379**(26): 2495–2505.

Pernik MN, Bird CE, Traylor JI, Shi DD, Richardson TE, et al. (2021). Patient-derived cancer organoids for precision oncology treatment. *J Pers Med* **11**(5): 423.

Ren X, Huang M, Weng W, Xie Y, Wu Y, et al. (2023). Personalized drug screening in patient-derived organoids of biliary tract cancer and its clinical application. *Cell Rep Med* **4**(11): 101277.

Qiao D, Wang RC, Wang Z (2025). Precision oncology: Current landscape, emerging trends, challenges, and future perspectives. *Cells* **14**(22): 1804.

Relling MV, Evans WE (2015). Pharmacogenomics in the clinic. *Nature* **526**(7573): 343–350.

Tilsed CM, Fisher SA, Nowak AK, Lake RA, Lesterhuis WJ (2022). Cancer chemotherapy: Insights into cellular and tumor microenvironmental mechanisms. *Front Oncol* **12:** 960317.

Trendowski MR, El Charif O, Dinh PC, Wheeler HE, Ardeshir-Rouhani-Fard S, et al. (2019). Genetic and modifiable risk factors contributing to cisplatin-induced toxicities. *Clin Cancer Res* **25**(4): 1147–1155.

Wang W, Gao M, Gao Y, Zheng H, Song N, et al. (2025). Integrating homologous recombination deficiency subtyping with TCGA molecular classification for enhanced prognostic stratification and personalised therapy in endometrial cancer. *Br J Cancer*.

Yang Z, Carrio-Cordo P, Baudis M (2024). Copy number variation heterogeneity reveals biological inconsistency in hierarchical cancer classifications. *Mol Cytogenet* **17:** 26.

Yi K, Park SH, Kim DU, Jeon DY, Lee HJ, et al. (2023). Patient-derived organoid model for predicting the chemoresponse in patients with colorectal cancer. *In Vivo* **37**(4): 1751–1759.

Zazuli Z, Vijverberg S, Slob E, Liu G, Carleton B, et al. (2018). Genetic variations and cisplatin nephrotoxicity: A systematic review. *Front Pharmacol* **9:** 1111.

Zhao L, Song L, Wang H, Tian W, Xi J, et al. (2025). Post-translational modification gene signature for treatment response in breast cancer. *Sci Rep* **15:** 23772.